# Improvement in Crystallization and Mechanical Properties of Poly(L-Lactide)-*b*-Poly(ethylene glycol)-*b*-Poly(L-Lactide) Bioplastic with Cerium Lactate

Arriya Chuangchai

A Thesis Submitted in Partial Fulfillment of Requirements for
degree of Master of Science in Chemistry
April 2025

# การปรับปรุงสมบัติการเกิดผลึกและสมบัติเชิงกลของพลาสติกชีวภาพชนิดพอลิแอลแลคไทด์-บล็อค-พอลิเอทิลีนไกลคอล-บล็อค-พอลิแอลแลคไทด์ด้วยซีเรียมแลคเตด

วิทยานิพนธ์

ของ

อาริยา ช่วงชัย



เสนอต่อมหาวิทยาลัยมหาสารคาม เพื่อเป็นส่วนหนึ่งของการศึกษาตามหลักสูตร

ปริญญาวิทยาศาสตรมหาบัณฑิต สาขาวิชาเคมี

เมษายน 2568

# Improvement in Crystallization and Mechanical Properties of Poly(L-Lactide)-*b*-Poly(ethylene glycol)-*b*-Poly(L-Lactide) Bioplastic with Cerium Lactate

Arriya Chuangchai

A Thesis Submitted in Partial Fulfillment of Requirements

for Master of Science (Chemistry)

April 2025

The examining committee has unanimously approved this Thesis, submitted by Miss Arriya Chuangchai , as a partial fulfillment of the requirements for the Master of Science Chemistry at Mahasarakham University

Examining Committee

.....Chairman
(Asst. Prof. Chanukorn Tabtimsai , Ph.D.)

.....Advisor
(Assoc. Prof. Yodthong Baimark , Ph.D.)

.....Committee
(Asst. Prof. Khongvit Prasitnok , Ph.D.)

.....Committee
(Assoc. Prof. Prasong Srihanam , Ph.D.)

Mahasarakham University has granted approval to accept this Thesis as a partial fulfillment of the requirements for the Master of Science Chemistry

.....
(Prof. Pairot Pramual , Ph.D.)
Dean of The Faculty of Science

.....
(Asst. Prof. Pondej Chaowarat , Ph.D.)
Dean of Graduate School

**TITLE** Improvement in Crystallization and Mechanical Properties of Poly(L-Lactide)-*b*-Poly(ethylene glycol)-*b*-Poly(L-Lactide) Bioplastic with Cerium Lactate

**AUTHOR** Arriya Chuangchai

**ADVISORS** Associate Professor Yodthong Baimark , Ph.D.

**DEGREE** Master of Science **MAJOR** Chemistry

**UNIVERSITY** Mahasarakham University **YEAR** 2025

## ABSTRACT

Plastic waste derived from petroleum-based plastics has become a significant environmental issue worldwide because of its non-biodegradability and high carbon footprint. Poly(L-lactide) (PLLA) has been the most considered substitute for petroleum-based plastics because of its biorenewability, biodegradability, and low carbon footprint. However, the low flexibility of PLLA compared to other commodity plastics has restricted its wider applications. PLLA-*b*-poly(ethylene glycol)-*b*-PLLA (PLLA-PEG-PLLA) triblock copolymer exhibited higher flexibility than the PLLA. In this study, the effect of the cerium lactate (Ce–LA) antibacterial agent on the crystallization, thermal decomposition, and mechanical properties of PLLA–PEG–PLLA was investigated. PLLA–PEG–PLLA/Ce–LA composites were prepared by a melt blending technique. The crystallisability, thermal stability, and tensile properties of the PLLA–PEG–PLLA were enhanced by the addition of Ce–LA. The crystallinity of the PLLA–PEG–PLLA matrix increased from 11.8% to 13.7-15.9%. The temperature at the maximum decomposition rate ($T_{d,\ max}$) of PLLA end-blocks increased from 310˚C to 311-327˚C. The ultimate tensile stress of the PLLA–PEG–PLLA matrix increased from 14.3 MPa to 15.1–19.5 MPa, while Young's modulus improved from 204 MPa to 230–312 MPa. This suggests that Ce–LA had potential for use as a nucleating, thermal stabilizing, and reinforcing agent for this flexible PLLA–PEG–PLLA bioplastic.

Keyword : bioplastic; polylactide; block copolymer; nucleating agent; reinforcing agent

# ACKNOWLEDGEMENTS

This thesis was gratefully acknowledged by the Center of Excellence for Innovation in Chemistry (PERCH-CIC). I am grateful to the Department of Chemistry, Faculty of Science, Mahasarakham University, for providing chemicals, instrumental support, and all other facilities.

I would like to express my sincere thanks to my thesis advisor, Assoc. Prof. Yodthong Baimark for his invaluable help and constant encouragement throughout the course of this research. I am most grateful for his teaching and advice, not only the research methodologies but also many other methodologies in life. I would not have achieved this far, and this thesis would not have been completed without all the support that I have always received from him.

I would like to acknowledge Asst. Prof. Chanukorn Tabtimsai, Assoc. Prof. Prasong Srihanam, and Asst. Prof. Khongvit Prasitnok for pieces of training valuable guidance and assistance in this research. Other former and current group members in the Biodegradable Polymers Research Unit, whom I do not mention by name, also deserve my deep appreciation.

I wish to express my sincere appreciation to Miss Yaowalak Srisuwan, Mr.Theeraphol Phromsopha, and all of my friends for their excellent assistance, encouragement, sincerity, and impression of friendship. Everything will always be in my mind.

Finally, I wish to express my heartfelt gratitude here to my Chuangchai family; and my beloved parents for their tender love, care, sacrifice, inculcation, and encouragement that found me to be a fortitude person.

Arriya Chuangchai

# TABLE OF CONTENTS

**Page**

# LIST OF TABLES

**Page**

# LIST OF FIGURES

**Page**

# CHAPTER I

# INTRODUCTION

## 1.1 Background

Nowadays, plastic waste from petroleum resources has become a serious environmental problem all over the world. The disposal of plastic waste is a serious environmental problem in modern times. There are two reasons why we must be aware of the use of renewable resources: 1) Environmental concerns in terms of the use of plastic waste are increasing, and global warming is a problem as a result. The release of carbon dioxide when plastic waste is burned, and 2) petroleum resources are limited and endless. As a result, in the future, the raw materials used to produce plastic will be less and gone. Therefore, researchers have turned to studying the raw materials used in plastic production that do not come from petroleum sources but come from natural sources that are renewable resources. This makes it possible to solve problems that will occur in the future [1, 2].

Biodegradable polymers can be defined as polymers that can be decomposed into simpler substances ($CH_4$, other inorganic compounds, $CO_2$, biomass, and water) under microbial enzymatic action [2]. Biodegradable polymers may be classified according to their chemical composition, origin, and method of synthesis. They can be divided into two main types: Natural and synthetic biopolymers, which are made from natural and petroleum resources, respectively, as shown in Figure 1.

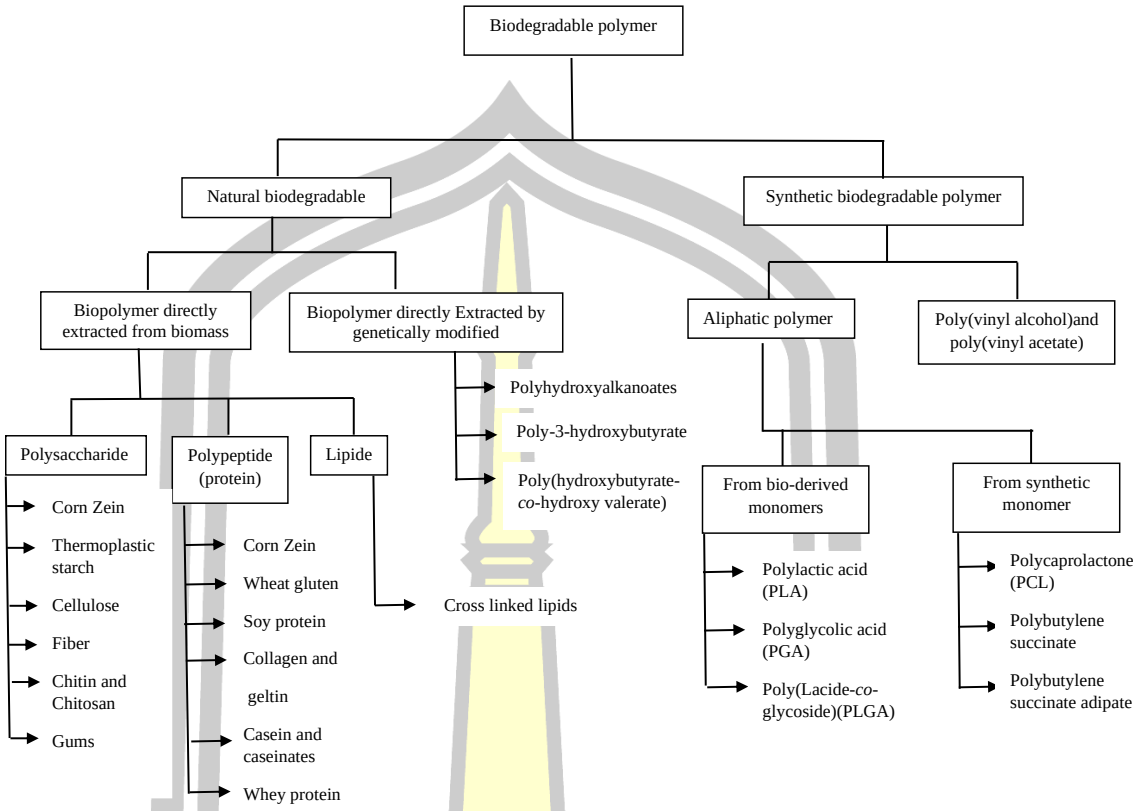


**Figure 1.** Classification of the main biodegradable polymers [2].

Natural biodegradable polymers (macromolecules composed of repeating structural units) are derived from renewable resources and can be broken down through natural processes into simpler compounds over time. Examples of natural biodegradable polymers include biopolymers directly extracted from biomass and biopolymers derived directly from naturally occurring or genetically engineered organisms. Biopolymers are directly extracted from biomass. Polysaccharides are major classes of biomolecules. They are long chains of carbohydrate molecules composed of several smaller monosaccharides. These complex bio-macromolecules function as an important source of energy in animal cells and form a structural component of a plant cell. The main source of polysaccharides is plant-based agricultural waste, where biopolymers such as cellulose, starch, and pectin are produced. Biopolymers are derived directly from naturally occurring or genetically engineered organisms. Microorganisms are a source of research on bioplastic

materials and biopolymers that use agricultural waste as a medium for growth. An example of microbiologically compounding plastic is polyhydroxyalkanoate (PHA) [2].

Synthetic biodegradable polymers are human-made polymers that are designed to break down into simpler compounds through natural processes over time. Aliphatic polyesters are synthesized from bio-derived monomers, including poly(lactic acid) (PLA), polyglycolic acid (PGA), and poly(lactide-*co*-glycolide) (PLGA). Aliphatic polyesters are synthesized from synthetic monomers (petroleum-based monomers) such as polycaprolactone (PCL), poly(butylene succinate) (PBS), and poly(butylene succinate adipate ) (PBSA) [4].

PLA is well-known for being a biodegradable and biocompatible polymer. It is synthesized from lactic acid obtained from renewable materials such as potato starch, wheat, rice bran, corn, and biomass. [3, 4]. Usually, lactic acid is produced by the fermentation of carbohydrates by lactic bacteria belonging mainly to the genus Lactobacillus, or fungi [5]. Lactobacillus is a bacteria that acts in the process of fermenting sugar into lactic acid, by converting sugar to lactic acid through the metabolic pathway. The lactic acid is used to form PLA through direct polycondensation as shown in Figure 2 (step 1) [6]. Low–molecular–weight PLA was then obtained.

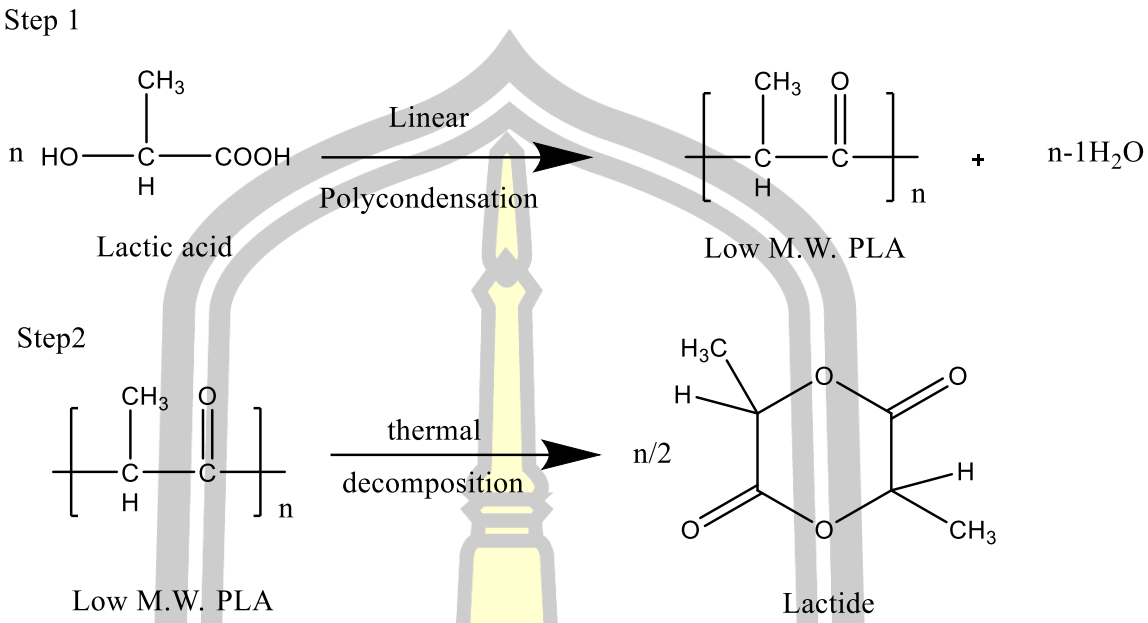


**Figure 2.** Synthesis of PLA by direct polycondensation (step 1) and lactide monomer by thermal decomposition (step 2) [7].

However, the resulting PLA has a low–molecular–weight (<10,000 g/mol) and low mechanical properties. This was due to the hydrolysis of a water by-product. High-molecular-weight PLA can be obtained by ring-opening polymerization of lactide monomers, which water by-products did not form. The lactide was synthesized through direct polycondensation of lactic acid, followed by thermal decomposition of the low–molecular–weight of PLA, as shown in Figure 2 (step 2). The polyester obtained from lactide was then called polylactide (PLA).

The main disadvantages of PLA are its brittleness and low heat resistance. The high glass transition temperature ($T_g$) of the PLA (~60°C) induced high brittleness. Plasticization effects can reduce PLA brittleness by decreasing the $T_g$ of PLA by the addition of a plasticizer [8]. Poly(L–lactide)–*b*–poly(ethylene glycol)–*b*–poly(L–lactide) (PLLA–PEG–PLLA) triblock copolymers were more flexible than PLLA [7]. The PEG middle blocks acted as plasticizing sites. Moreover, the PLA showed a very

slow crystallization rate after the melt process. The low crystallinity of PLA gave it low heat-resistant properties. The crystallinity of PLA has been improved by the addition of nucleating agents [4].

**1.2 Research objectives**

1.2.1 To synthesize and characterize the cerium lactate (Ce–LA).

1.2.2 To prepare the PLLA–PEG–PLLA/Ce–LA composites by melt blending.

1.2.3 To study the crystallization and mechanical properties of PLLA–PEG–PLLA /Ce–LA composites by various analytical techniques.

**1.3 Expected results obtained from the research**

The Ce–LA powder can be synthesized.

The triblock copolymer of PLLA–PEG–PLLA can be synthesized.

The effects of Ce–LA content on the thermal and mechanical properties of PLLA–PEG–PLLA were obtained.

**1.4 Scopes of Research**

1.4.1 Ce–LA was synthesized from $Ce(NO_3)_3$ and sodium lactate.

1.4.2 Ce–LA was characterized by scanning electron microscopy (SEM). X-ray diffractometry (XRD) and Thermogravimetric analysis (TGA).

1.4.3 PLLA–PEG–PLLA was synthesized using PEG as an initiator and stannous octoate as a catalyst. The PEG middle-block length was 20,000 g/mol. The PLLA block lengths were around 50,000 g/mol on both sides.

1.4.4 PLLA–PEG–PLLA was characterized by proton nuclear magnetic resonance ($^1$H–NMR) spectroscopy, gel permeation chromatography (GPC), differential scanning calorimetry (DSC), and TGA.

1.4.5 PLLA–PEG–PLLA/Ce–LA composites were prepared by melt blending. Composite films were prepared by compression molding.

1.4.6 PLLA–PEG–PLLA/Ce–LA composites were characterized by XRD, DSC, SEM, TGA, and tensile test.

**1.5 Research Places**

SC1 - 406, Department of Chemistry, Faculty of Science, Mahasarakham University.

SC2 - 210, Department of Chemistry, Faculty of Science, Mahasarakham University.

# CHAPTER II

# LITERATURE REVIEW

## 2.1. PLLA–PEG–PLLA copolymers

Poly(lactic acid) or PLA is a synthetic biodegradable polyester widely utilized in various applications, ranging from everyday domestic life uses to academic and industrial purposes. Besides its renewable and sustainable character, PLA's selection can also be attributed to its superior performance, such as excellent mechanical properties, relatively to other polymers, low glass transition temperature (45–70 °C), and melting point (140–190 °C). This combination of characteristics makes PLA an almost ideal material, which can be processed at a low economic cost, whereas it serves well within the modern framework of green and circular economies [11]. However, the disadvantages of low flexibility and the slow crystallization rate of PLLA limit its wider applications. PLLA is a rather brittle and rigid polymer. While PLA has a glass transition temperature well above room temperature and is amorphous at room temperature, the elongation ratio is only about 5%. Crystallinity, if developed, increases the elastic modulus and further enhances the brittleness [12, 13]. Considerable efforts have been made to improve the mechanical properties of PLA, such as blending, copolymerization, and plasticization [14,15].

Block copolymers are polymers formed by alternating chain segments with different chemical structures that can be used as blending compatibilizers and interfacial modifiers [16]. Block copolymers with blocky structures: PLA–*b*–PEG–*b*–PLA is a biodegradable triblock copolymer (Figure 3) that presents both the high mechanical properties of PLA and the hydrophilicity of PEG [17].

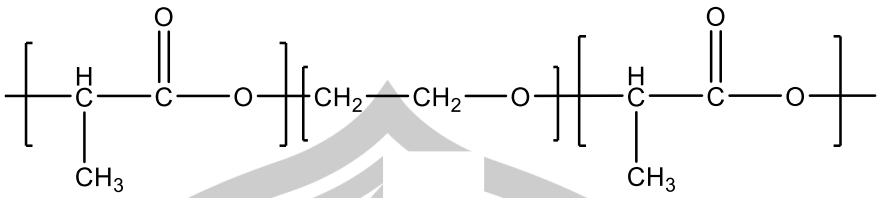

**Figure 3.** Chemical structure of PLA–PEG–PLA [18].

Plasticizers are chemicals added to plastics to increase the flexibility and softness of the material. In general, plastics are firm, but adding plasticizers makes the plastic more flexible, reducing durability and giving a soft appearance. Benefits of using plasticizers: (1) Flexibility: plasticizers help to reduce the strength of plastic, making the material more flexible, making it easier to shape and use. (2) Softness: plasticizers soften plastic, making it uniform and smooth. (3) Temperature resistance: adding plasticizers can make plastics more resistant to high or low temperatures. (4) Prevents plastic breakage: plasticizers reduce plastic breakage, making it more flexible without having to bite hard. (5) Increases Viscosity: plasticizers increase the viscosity and flexibility of plastics, making them ideal for manufacturing products that require flexibility [19]. The PLA was plasticized with various plasticizers and their efficiency was evaluated in two aspects: one is the shift of glass transition temperature ($T_g$) to lower temperatures, and the other is the improvement of mechanical properties of poly(propylene glycol) (PPG) and poly(ethylene glycol) (PEG) were found to be efficient plasticizers for PLA. The tensile strength and elongation of the blend films increased at low PEG concentration, whereas tensile strength decreased, and elongation increased at high PEG concentration, indicating an improvement in the ductility of PLA [19].

Table 1 shows the composition and sample codes of PLA/PEG blend films of different MWs. Molecular weights of the PEG were 4000, 20,000, and 35,000 g/mol, respectively.

**Table 1.** Compositions and sample codes of PLA/PEG blend films of different MWs [19].

| Sample code | MW of PEG (g/mol) | Composition (wt%) | | |
|---|---|---|---|---|
| | | PLA | PEG | Total |
| Pure PLA | – | 100 | 0 | 100 |
| PLA–G4-5% | 4000 | 95 | 5 | 100 |
| PLA–G4-10% | | 90 | 10 | 100 |
| PLA–G4-20% | | 80 | 20 | 100 |
| PLA–G20-5% | 20,000 | 95 | 5 | 100 |
| PLA–G20-10% | | 90 | 10 | 100 |
| PLA–G20-20% | | 80 | 20 | 100 |
| PLA–G35-5% | 35,000 | 95 | 5 | 100 |
| PLA–G35-10% | | 90 | 10 | 100 |
| PLA–G35-20% | | 80 | 20 | 100 |

The effects of PEG MW and concentration on the thermal properties of the PLA/PEG blend films were investigated through DSC. In general, the thermal behavior of a polymer blend strongly depends on its composition and chemical interactions. The $T_g$ values decreased steadily as the PEG ratio increased. The elongation at break of the PLLA blend films also increased with the PEG blend ratio as shown in Figure 4 and Table 2. However, as the MW of PEG decreased, its polarity increased because of the large number of terminal hydroxyl groups in PEG. This leads to the augmentation of the rotational barrier of the backbone chains, making the chain stiffer [19].

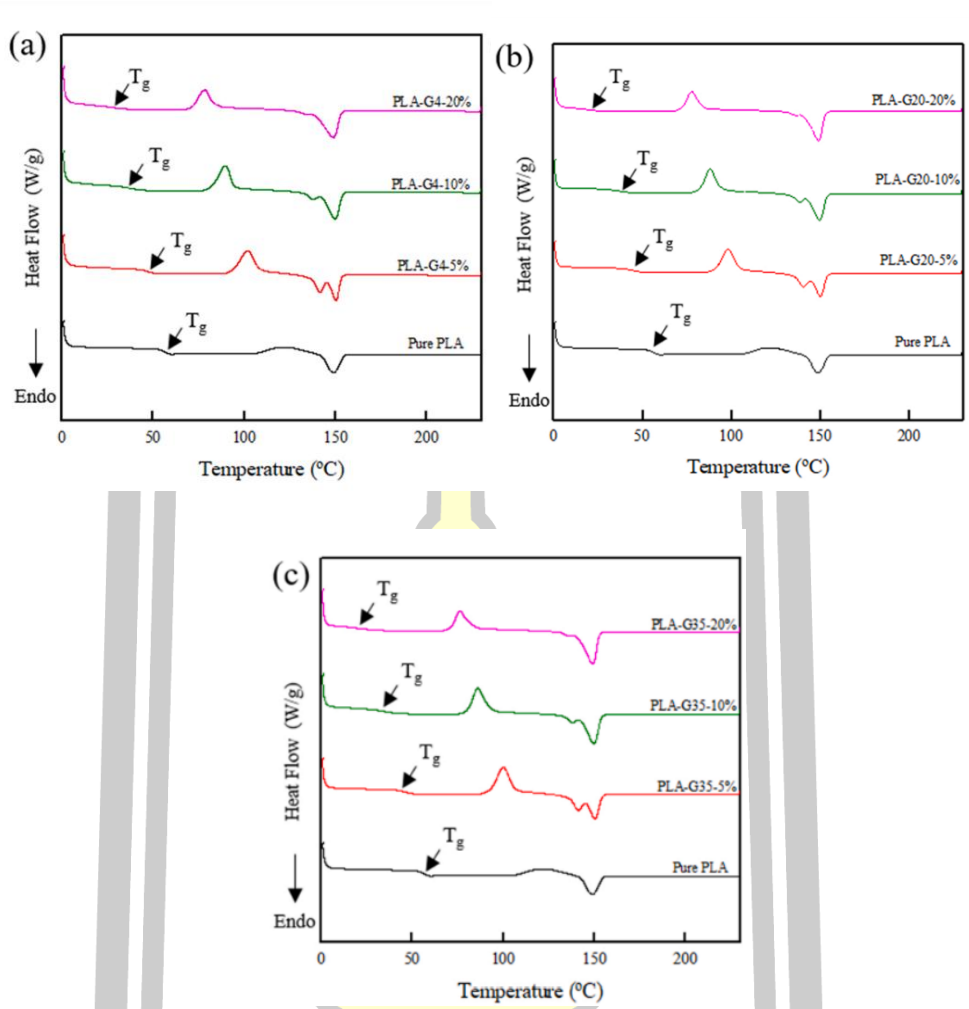


**Figure 4.** Effect of PEG blend ratio on the $T_g$ of the PLA phases (a) PLA–G4, (b) PLA–G20, and (c) PLA–G35 [19].

**Table 2.** Thermal properties of the PLA and PLA/PEG blend films [19].

| Sample code* | $T_g$ of PLLA phases (°C) |
|---|---|
| Pure PLA | 56.9 |
| PLA–G4–5% | 47.2 |
| PLA–G4–10% | 36.5 |
| PLA–G4–20% | 24.7 |
| PLA–G20–5% | 45.3 |
| PLA–G20–10% | 36.2 |
| PLA–G20–20% | 18.5 |
| PLA–G35–5% | 46.4 |
| PLA–G35–5% | 34.2 |
| PLA–G35–20% | 19.6 |

*G4, G20, and G35 are PEG with molecular weights of 4000, 20,000, and 35,000 g/mol, respectively.

The tensile strength and Young's modulus of pure PLA remained constant or increased slightly when 5 wt% PEG was added and then decreased with increasing PEG concentration as shown in Figure 5.

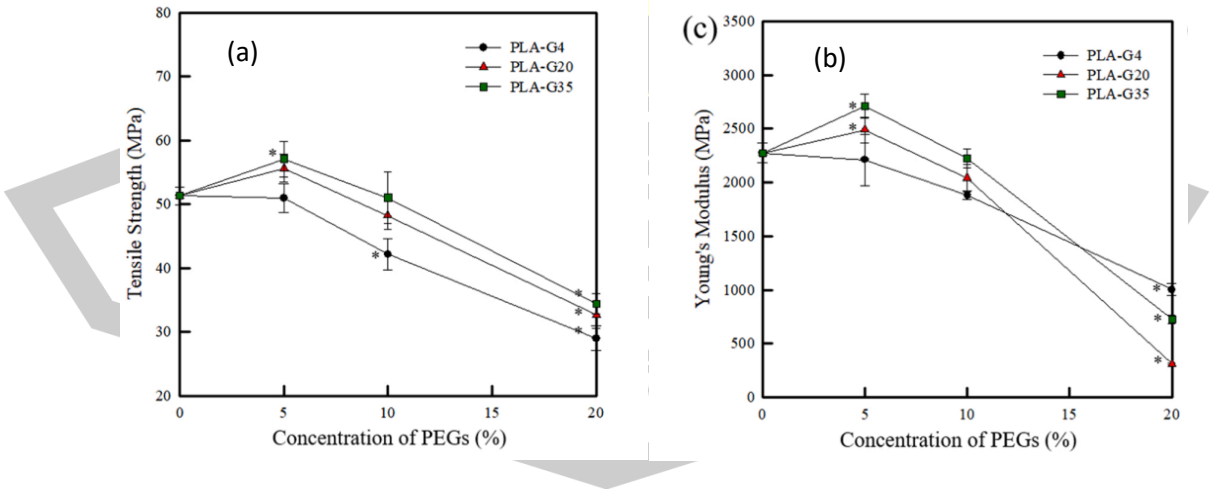


**Figure 5.** (a) Stress in the yield point and (b) Young's modulus of pure PLA and PLA/PEG blend films [19].

Furthermore, Figure 6 shows that the PLA/PEG blend films with 20 % PEG have a high elongation at break values ($p < 0.05$), which became more apparent with high MW PEG. The mechanical properties of the PLA–PEG blend films could be related to the change in crystallinity and the existence of intermolecular forces between PLA–PLA and PEG–PEG. At a low PEG concentration, the plasticizing effect of PEG might not be dominant, whereas the intermolecular interactions between the PLA chains might be strong. However, with increasing concentrations of plasticizing PEG, the intermolecular forces between the PLA chains weakened, whereas those between PEG and the PLA chains strengthened Consequently, the PLA/PEG blend films with high PEG concentrations became softer.

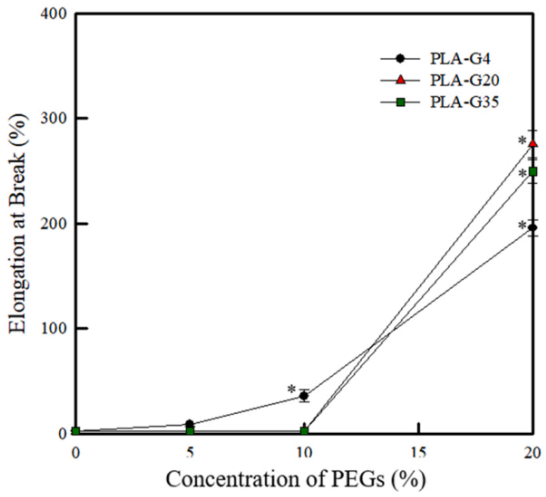


**Figure 6.** Elongation at break of pure PLA and PLA/PEG blend films. The values marked with the asterisk (*) showed statistically significant differences compared to pure PLA ($p < 0.05$) [19].

PEG was considered a good plasticizer for PLA, crystallization behavior, melting behavior and its application in drug release of PLA–PEG diblock or triblock copolymers have always been investigated in most works. Triblock copolymers of PLLA–PEG–PLLA were synthesized by ring-opening polymerization using $Sn(Oct)_2$ as a catalyst. The 1-dodecanol and PEG were used as initiators for preparing the PLLA and PLLA–PEG–PLLA, respectively. Feed molecular weights of PLLA and

PLLA–PEG–PLLA were approximately 100,000 and 120,000 g/mol, respectively [20].

The effects of PEG with and without chain extenders on the mechanical properties of the PLLA and PLLA–PEG–PLLA are illustrated in Figure 7. The PLLA–PEG–PLLA films showed higher strain at break than those of the PLLA films suggesting they were more flexible than the PLLA films. Moreover, yield points were detected for all the PLLA–PEG–PLLA films due to the plasticization effect of PEG blocks. In addition, stress at yield of the chain-extended PLLA–PEG–PLLA films was higher than the non-chain-extended PLLA–PEG–PLLA film being 23.8–27.4 MPa and 14.5 MPa, respectively. The chain extension reaction can improve the stress at yield of PLLA–PEG–PLLA films [20].

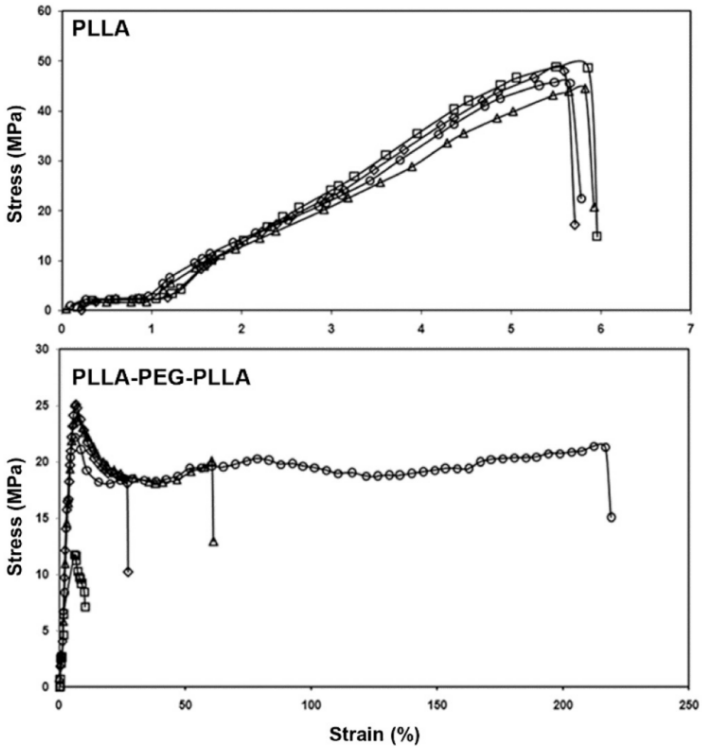


**Figure 7.** Tensile curves of (above) PLLA and (below) PLLA–PEG–PLLA films (□) without chain extender and with chain extender contents of (◇) 1.0, (Δ) 2.0 as well as (o) 4.0 phr [20].

The PLLA–PEG–PLLA films exhibited lower stress at break and Young's modulus as well as higher strain at break than those of the PLLA films shown in Figure 8. This could be explained by the flexibility of PEG blocks decreasing $T_g$ of the PLLA blocks thereby enhancing the durability of PLLA–PEG–PLLA films during tensile deformation. The stress and strain at the break of PLLA–PEG–PLLA films increased with the content of the chain extender [20].

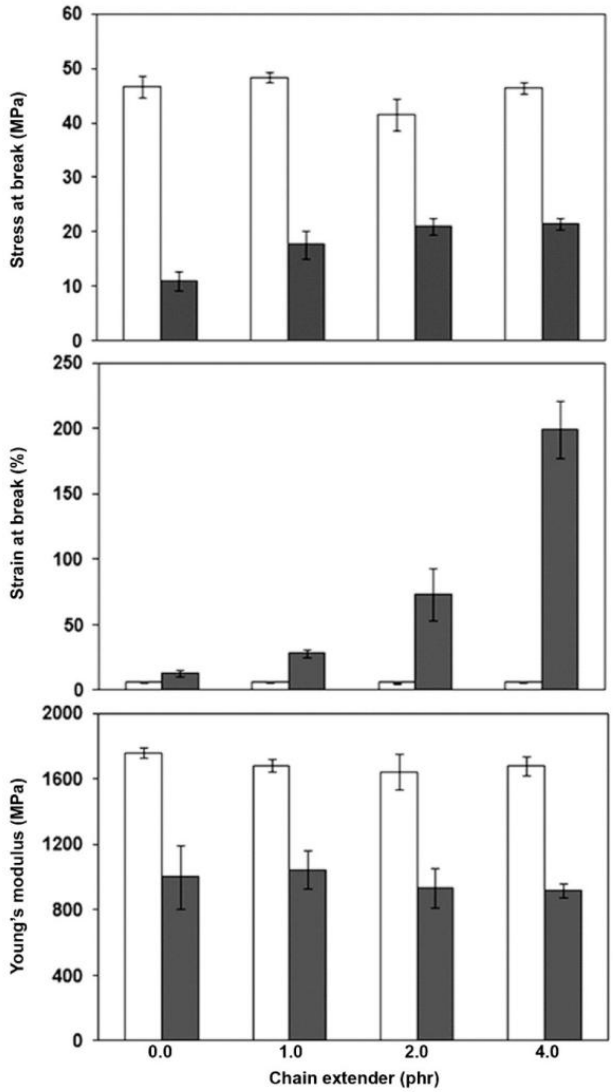


**Figure 8.** Tensile properties of (□) PLLA and (■) PLLA–PEG–PLLA films with various chain extender contents [20].

From the results of $X_{c,\,XRD}$ in Figure 9, the crystallinities of PLLA–PEG–PLLA decreased (amorphous phase increased) when the contents of the chain extender were increased. This enhances the chain mobility of the PEG blocks to induce a plasticization effect. The PLLA–PEG–PLLA films with and without chain extension had similar Young's modulus in the range of 916–1046 MPa. The results indicate that the long-chain branched structures of chain-extended PLLA–PEG–PLLA films improved the stress and strain at break as well as stress at yield by chain entanglement in amorphous regions.

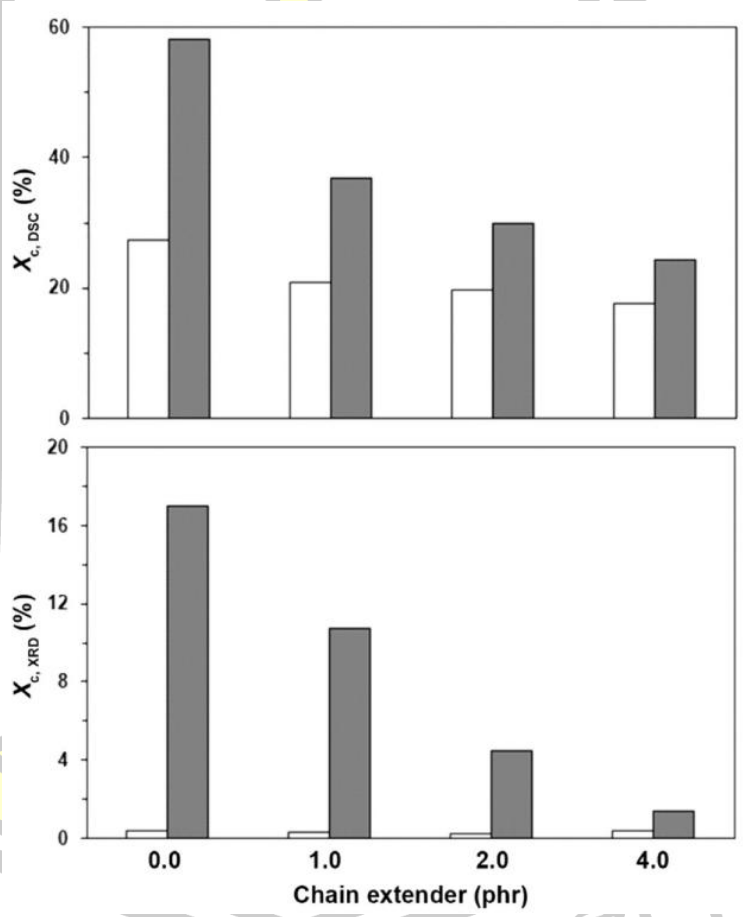


**Figure 9.** $X_{c,\,DSC}$ (above) and $X_{c,\,XRD}$ (below) of PLLA and PLLA–PEG–PLLA films with various contents of the chain extender [20].

## 2.2 Reinforcing agents

"Reinforcing agents" or "reinforcers" in a polymer refers to a material that is added to a polymer to increase the strength, durability, or other properties of the polymer material.

Examples of reinforcing agents used in polymers include:

1. Glass Fibers: Glass fibers are used as reinforcement in polymers to increase strength and durability.
2. Carbon Fibers: Carbon fibers are a reinforced material with very high strength and durability, often used in polymers that require additional strength.
3. Chlorinated Polymers: Adding chlororide to a polymer increases its resistance to environmental conditions.
4. Alloying: Mixing polymers with other materials to enhance their properties in various ways.
5. Silica or Silicate: Adding silica or silicate to a polymer increases its strength and resistance to pressure.

Typical reinforcing agents for PLLA–PEG–PLLA triblock copolymers are microcrystalline cellulose (MCC) [21], boron nitride [22], and Polysorb$^{TM}$ [23]. More detail has described as follows.

### 2.2.1 Microcrystalline cellulose (MCC)

Microcrystalline cellulose (MCC) is a bio-filler for the development of polymer-based composites. MCC showed low density, strong mechanical properties, high crystallinity, non-toxic, renewability, biodegradability, and low cost when it was prepared by removing the amorphous phase of purified cellulosic fibers via acid hydrolysis. the addition of MCC improved the thermal stability of the PLLA [21].

Typical tensile curves of the biocomposite films are shown in Figure 10. Strain at the break for all the PLLA–PEG–PLLA /MCC biocomposite films in Figure 10 (below) were largely higher than the PLLA/MCC biocomposite films in Figure 10 (above).

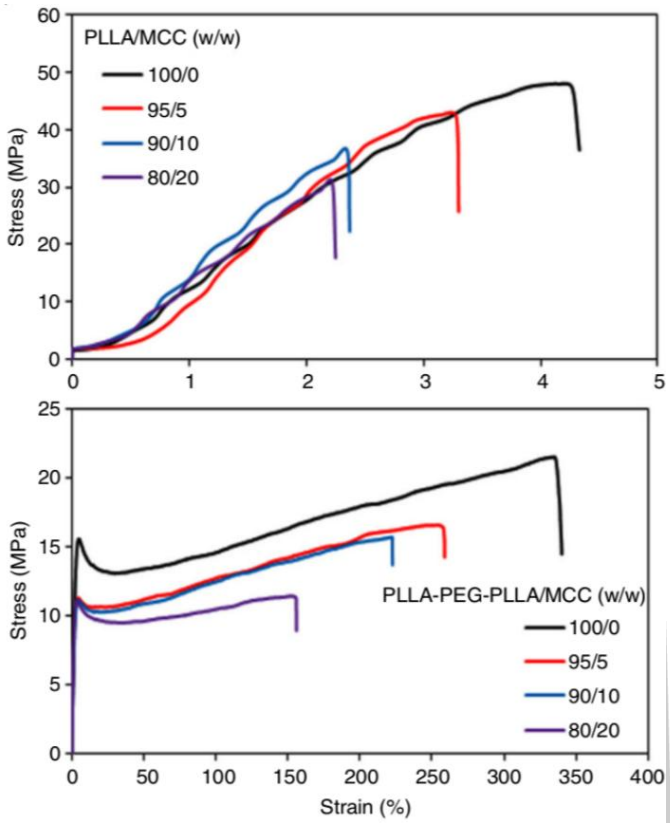


**Figure 10.** Tensile curves of (above) PLLA/MCC and (below) PLLA–PEG–PLLA/MCC biocomposite films with various MCC contents [21].

The results indicated that all the PLLA–PEG–PLLA/MCC biocomposite films were more extensible than those of the PLLA/MCC biocomposite films. The flexible PEG middle blocks enhanced the extensibility of PLLA–PEG–PLLA/MCC biocomposite films. The averaged tensile properties are summarized in Tables 3 and 4 for PLLA/MCC and PLLA–PEG–PLLA composites, respectively.

**Table 3.** Averaged tensile properties of PLLA/MCC and PLLA–PEG–PLLA/MCC biocomposite [21].

| Biocomposite films | PLLA/MCC (w/w) | | | | |
|---|---|---|---|---|---|
| | Stress at yield (MPa) | Strain at yield (%) | Stress at break (MPa) | Strain at break (%) | Young's modulus (MPa) |
| 100/0 | – | – | 43.9 ± 3.1 | 4.2 ± 0.6 | 1466 ± 101 |
| 95/5 | – | – | 41.3 ± 4.1 | 3.3 ± 0.2 | 1530 ± 92 |
| 90/10 | – | – | 37.1 ± 2.1 | 3.2 ± 0.1 | 1559 ± 89 |
| 80/20 | – | – | 31.5 ± 1.6 | 2.0 ± 0.2 | 1749 ± 104 |

**Table 4.** Averaged tensile properties of PLLA–PEG–PLLA/MCC biocomposite [21].

| Biocomposite films | PLLA–PEG–PLLA/MCC (w/w) | | | | |
|---|---|---|---|---|---|
| | Stress at yield (MPa) | Strain at yield (%) | Stress at break (MPa) | Strain at break (%) | Young's modulus (MPa) |
| 100/0 | 15.6 ± 3.2 | 4.9 ± 1.2 | 19.9 ± 1.4 | 374.6 ± 43.0 | 672 ± 63 |
| 95/5 | 11.3 ± 1.1 | 4.3 ± 0.9 | 15.6 ± 1.0 | 255.0 ± 21.5 | 696 ± 54 |
| 90/10 | 11.1 ± 2.4 | 4.9 ± 1.4 | 15.1 ± 0.5 | 224.6 ± 9.80 | 726 ± 78 |
| 80/20 | 10.2 ± 2.8 | 4.6 ± 1.5 | 12.2 ± 0.5 | 161.5 ± 13.9 | 798 ± 68 |

The stress and strain at break of both PLLA and PLLA–PEG–PLLA films decreased steadily when the MCC was blended at increasing content. The stress at yield of the PLLA–PEG–PLLA/MCC biocomposite films also decreased as the MCC content increased but the strain at yield did not change in trend. The agglomeration of MCC and poor matrix-MCC adhesion caused decreases in stress and strain at the break of the biocomposite films. The results indicated that the interfacial adhesion on PLLA–PEG–PLLA/MCC biocomposites was not strong enough to enhance stress transfer from PLLA–PEG–PLLA matrix to the MCC particle surfaces to improve the stress at the break of the biocomposite films. Young's modulus of the biocomposite films increased with the MCC content. This is due to the high crystallinity of MCC inducing an increase of the Young's modulus of the biocomposite films. However, from the results of tensile properties, the PLLA–PEG–PLLA/MCC biocomposites still

exhibited higher flexibility than those of the PLLA/MCC biocomposites for all the MCC contents [21].

### 2.2.2 Boron Nitride

Boron nitride (BN) is a remarkable nanomaterial that has gained considerable attention in polymer nanocomposites due to its exceptional thermal conductivity, dielectric properties, mechanical strength, and chemical and thermal stability. Its versatility makes it a valuable component for enhancing the performance of polymers in various industries and applications. Various reinforcing fillers such as natural fibers, nano clay, cellulose nanocrystals, and BN have been used to improve the mechanical strength of PLLA. Among these fillers, BN powder is one of the most interesting reinforcing fillers because of its good thermal and chemical stability, low reactivity, and high mechanical strength. Moreover, BN powder enhanced the crystallization of PLLA and poly(3-hydroxybutyrate) (PHB) by acting as a heterogeneous nucleating agent [22].

Figure 11 presents typical tensile curves of pure PLLA–PEG–PLLA and its composite films. The averaged tensile properties are summarized in Table 5.

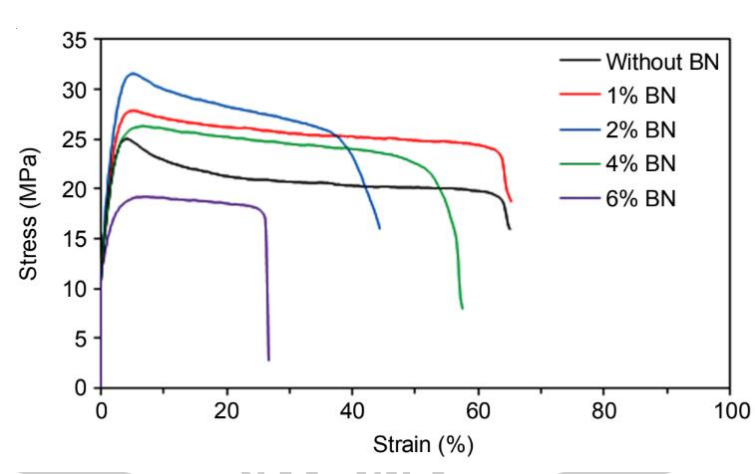


**Figure 11.** Typical tensile curves of PLLA–PEG–PLLA/BN films with various BN contents [22].

**Table 5.** Averaged tensile properties of PLLA–PEG–PLLA/BN films [22].

| BN content (wt%) | Ultimate tensile stress (MPa) | Strain at break (%) | Young's modulus (MPa) |
|---|---|---|---|
| – | 25.0 ± 2.4 | 76 ± 12 | 187 ± 21 |
| 1 | 27.8 ± 2.6 | 70 ± 11 | 229 ± 18 |
| 2 | 31.6 ± 1.8 | 64 ± 9 | 294 ± 28 |
| 4 | 26.3 ± 3.9 | 42 ± 15 | 207 ± 45 |
| 6 | 19.2 ± 4.1 | 24 ± 18 | 104 ± 37 |

The ultimate tensile stress and Young's modulus of the composite films increased while strain at break decreased when the BN content increased up to 2 wt%. These results indicated that the BN particles induced a reinforcing effect on PLLA–PEG–PLLA films. The composite films with 1 and 2 wt% BN showed a yield point indicating that they were flexible. The results suggested that interfacial adhesion on PLLA–PEG–PLLA/BN composites was strong enough to enhance stress transfer from the PLLA–PEG–PLLA matrix to the boron nitride particle surfaces to increase the tensile stress and Young's modulus of the composite films [22].

The ultimate tensile stress and Young's modulus of the composite films decreased when the BN content was higher than 2 wt%. This can be explained by the aggregation of BN particles in the PLLA–PEG–PLLA matrices as previously described from the SEM analysis. Aggregation of reinforced fillers reduced the mechanical properties of the polymer composites because of decreased surface areas for stress transfer of fillers. However, these PLLA–PEG–PLLA/BN composite films were still more flexible than the pure PLLA films (5-10% strain at break) [22].

## 2.3 Nucleating agents

Nucleating agents are inorganic materials added to polymers to increase the crystallinity and shorten the crystallization times (Figure 12). They speed up the transition from melt to solid material. Changing the crystallinity of plastics changes the properties such as density and clarity. Nucleating agents are used in a combined form with the cooling gradient imposed on the biopolymer during its final processing stage, according to the desired crystalline morphology and degree of crystallinity. Typical nucleating agents for aliphatic polyesters, such as PLA, include talc powder [24], calcium carbonate [25], acrylonitrile butadiene styrene (ABS) [26], zinc phenylphosphonate (PPZn) [27], dimethyl 5-sulfoisophthalic acid potassium salt, LAK-301 [28], and titanium oxide [29].

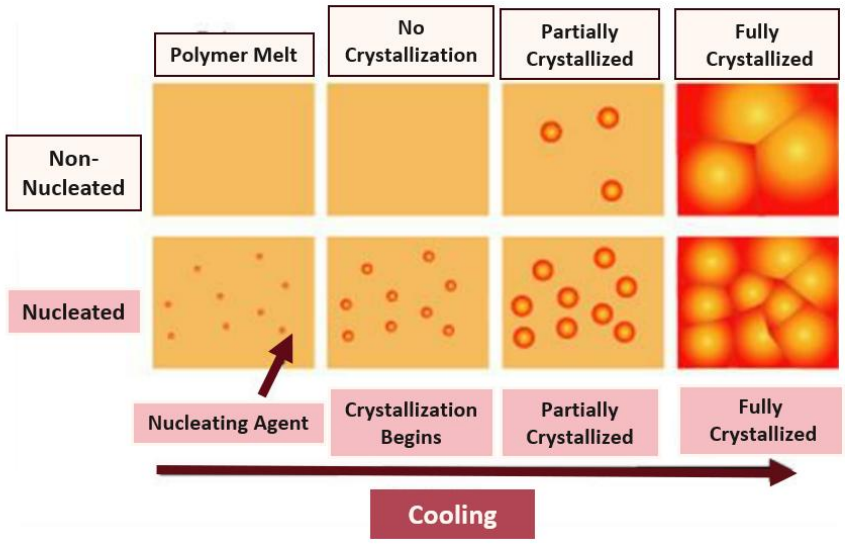


**Figure 12.** Illustration of the crystallization process in non-nucleated and nucleated matrix [30].

### 2.3.1 Zinc phenyl phosphonate (PPZn)

Zinc phenylphosphonate (PPZn), one of the most famous nucleation agents, has a layered structure like montmorillonite clay, and it can significantly increase the crystallization rate of PLA [27]. The effect of PPZn concentration on the non-isothermal crystallization of PLA was measured by DSC. As shown in Figure 13(a)

and Table 6, the exothermic melt crystallization peak ($T_{mc}$) of $PLA_{am}$ is not detected upon cooling at 10 ˚C/min because its crystallization rate is too slow to reach completion. In contrast, an exothermic cold crystallization peak ($T_{cc}$) (114.2 ˚C) is observed in the subsequent re-heating process [Figure 13(b)] [27].

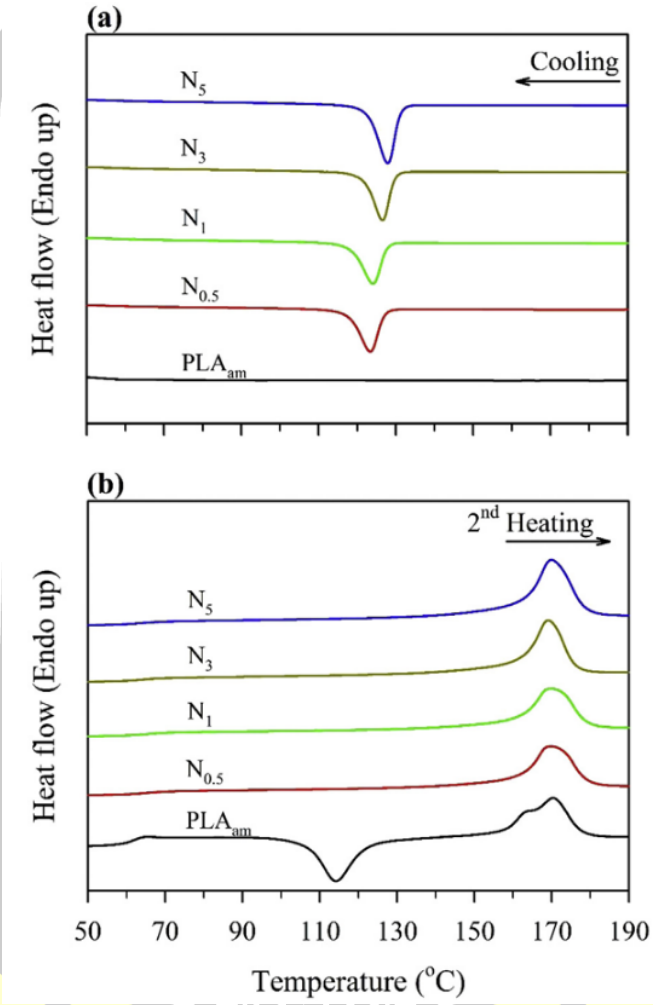


**Figure 13.** DSC curves recorded during (a) the cooling period at 10 ˚C/min and (b) the subsequent heating processes at 20 ˚C/min for PLA/PPZn blends with different PPZn concentrations [27].

**Table 6.** Non-isothermal and isothermal crystallization of amorphous PLA and PLA/PPZn blends [27].

| Sample code | PPZn (wt%) | Cooling | | | Heating | | | $t_{1/2}$ (min) |
|---|---|---|---|---|---|---|---|---|
| | | $T_{mc}$ (°C) | $\Delta H_c$ (J/g) | $X_{mc}$ (%) | $T_{cc}$ (°C) | $\Delta H_{cc}$ (J/g) | $X_{cc}$ (%) | |
| PLA | 0 | ND | ND | ND | 114.2 | 50.2 | 54.0 | 28.1 |
| $N_{0.5}$ | 0.5 | 123.4 | 54.4 | 58.7 | ND | ND | ND | 0.8 |
| $N_1$ | 1.0 | 124.1 | 54.2 | 58.8 | ND | ND | ND | 0.8 |
| $N_3$ | 3.0 | 126.5 | 56.8 | 63.0 | ND | ND | ND | 0.6 |
| $N_5$ | 5.0 | 127.9 | 59.5 | 67.3 | ND | ND | ND | 0.5 |

With 0.5 wt% PPZn, the crystallization of PLA/PPZn blend ($N_{0.5}$) is completed upon cooling, and its $T_{mc}$ is 123.4℃. With increasing PPZn concentration, the $T_{mc}$ becomes sharp and subsequently shifts to a higher temperature. Upon the addition of 5 wt% PPZn, the $T_{mc}$ of the PLA/PPZn blend ($N_5$) increased to 127.9℃. These results indicate that not only does the crystallization rate of PLA become faster but also the $T_{mc}$ value increases when the PPZn loading in the PLA matrix is increased. Generally, the crystals formed at higher $T_{mc}$ have larger lamellar thickness; thus, they possess a higher degree of crystallinity ($X_{mc}$) [27]. The crystallinities of annealed PLA and PLA/PPZn blends were investigated by XRD as shown in Figure 14(a) [27].

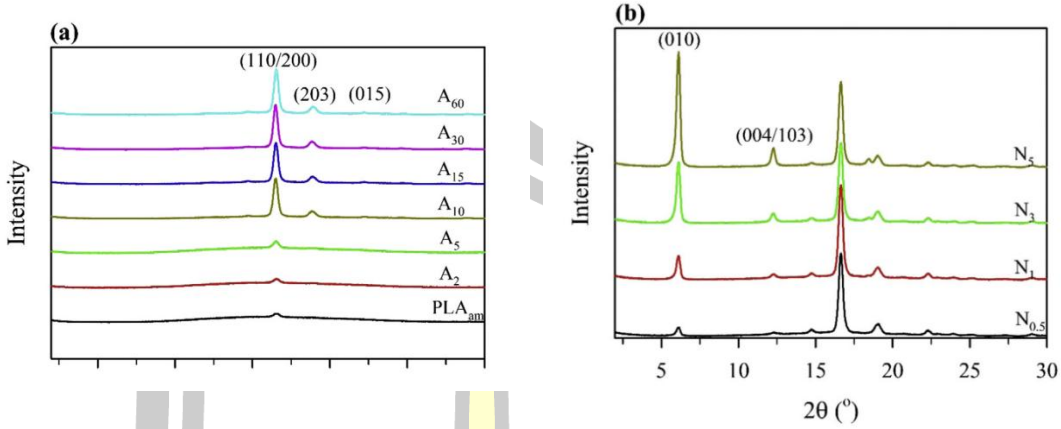


**Figure 14.** The XRD patterns of (a) amorphous PLA with various annealing times at 110˚C and (b) the PLA/PPZn blends with different PPZn concentrations [27].

Figure 14(b) shows the XRD patterns of the PLA with various annealing times at 110˚C. In addition to a sharp diffraction peak at 16.5˚(110/200 lattice planes), two noticeable small peaks were also observed at 18.9˚(203 lattice plane) and 22.3˚(015 lattice plane) after 10 min of annealing [27] and the intensity increased with increasing annealing time, which was likely caused by the development of ordered crystallites and the formation of crystalline structures throughout the annealing process. On the other hand, the XRD patterns of the PLA with various amounts of PPZn are shown in Figure 14(b) [27].

The diffraction peaks of crystallized PLA between 15˚and 25˚ two additional diffraction peaks were observed for all the PLA/PPZn blends. The diffraction peaks at 6.1˚and 12.3˚were attributed to the diffraction from the (010) and (004/103) lattice planes of PPZn, respectively, and the intensity of these peaks increased considerably with increasing PPZn concentration [27].

2.3.2 LAK-301

LAK–301 was used to mix with PLA to increase the crystallinity of PLA because LAK–301 has outstanding properties in improving the polymer by adding crystallinity to PLA. Figure 15 shows the crystallinity calculated according to DSC data. For PLA composites with added NA, the crystallinity increased more than that of P-NA0-NF. The size of the PLA crystal becomes smaller as the NA is added;

however, the crystallinity did not increase for P–NA6–NF even when 6 phr NA was added. Thus, there is a critical minimum concentration of the NA. Above this concentration, there is no significant change in the crystallization rate due to the motion of the NA. In this study, the economical amount of the NA to be added for PLA crystallization was determined to be 2 phr [28].

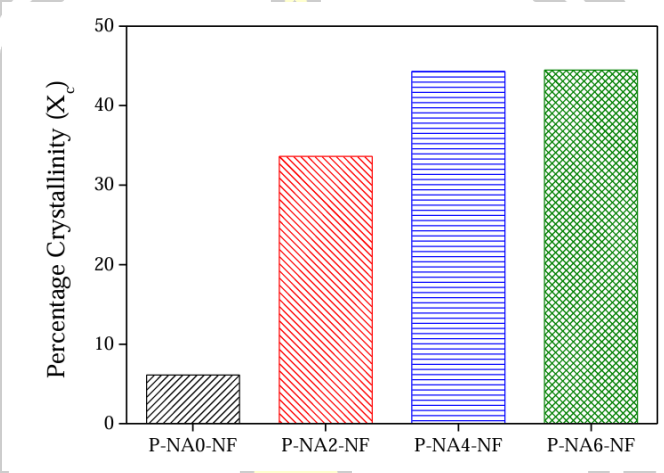


**Figure 15.** Percentage crystallinity of the NF-reinforced PLA composites with different NA contents [28].

2.3.3 Cerium lactate

Cerium is a rare earth element with variable valency, commonly found in either the +3 or +4 oxidation state. Lactic acid, on the other hand, is an organic acid with the formula $C_3H_6O_3$. The specific formula for cerium lactate will depend on the valency of cerium in this compound."cerium lactate" (Ce–LA) refers to a chemical compound that contains cerium in combination with lactic acid. The chemical formula for cerium lactate can be determined based on the valency of cerium and lactic acid as shown below in Figure 16.

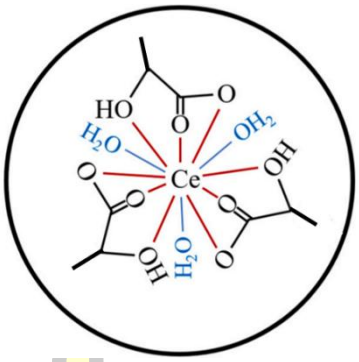


**Figure 16.** The chemical formula for cerium lactate [31].

Cerium lactate was synthesized to improve the properties of PLA. $Ce(NO_3)_3$ and sodium lactate were dissolved in deionized water and then mixed in a flask with a molar ratio of 1:3. After stirring at 35 ˚C for 4 h, ammonia was added to adjust the pH to 7, and the solution was allowed to stand for 12 h. Finally, the sediment was centrifuged and filtered, and then dried at 100 ˚C in a vacuum oven for 12 h to obtain Ce–LA. It showed that Ce–LA not only significantly improved the crystallizability and also imparted the antibacterial ability to PLLA. This study provides a beneficial solution for the development of PLA materials with high crystallinity and antibacterial properties [31].

Adding corresponding functional additives is an effective way to improve the performance of PLLA–PEG–PLLA. To adjust the crystallinity of PLLA-PEG-PLLA, many researchers have utilized nucleating agents to achieve this effect [30]. Using Ce-LA as a crystallizing agent for PLA, when the content of Ce–LA in PLA was 0.9 wt%, the crystallinity was 39.35%, which was 77% higher than that of pure PLA, as shown in Table 7 [31].

**Table 7.** Percentage of crystallinity of PLA/Ce-LA films [31].

| Sample | $X_c$ (%) |
|---|---|
| PLA/Ce-LA 0 | 22.17 |
| PLA/Ce-LA 3 | 35.87 |
| PLA/Ce-LA 6 | 39.35 |
| PLA/Ce-LA 9 | 39.35 |
| PLA/Ce-LA 12 | 37.93 |
| PLA/Ce-LA 18 | 37.31 |
| PLA/Ce-LA 25 | 35.48 |

The promoting effect of Ce–LA on the crystallization of PLA mainly comes from three aspects. First, the lactic acid ligand in Ce–LA is an organic small molecule with a good affinity for PLA, which is conducive to the crystallization of PLA by adhering the macromolecular chain of PLA to the lactic acid ligand. Second, the rare earth cerium in Ce–LA has a strong coordination effect with oxygen in PLA, and rare earth cerium ions have a high coordination number and interact with PLA molecules to enhance crystallinity. Third, Ce–LA, as a foreign substance, can play a role as a heterogeneous nucleating agent in PLA to promote the crystallization of PLA, as shown in Figure 17 [31].

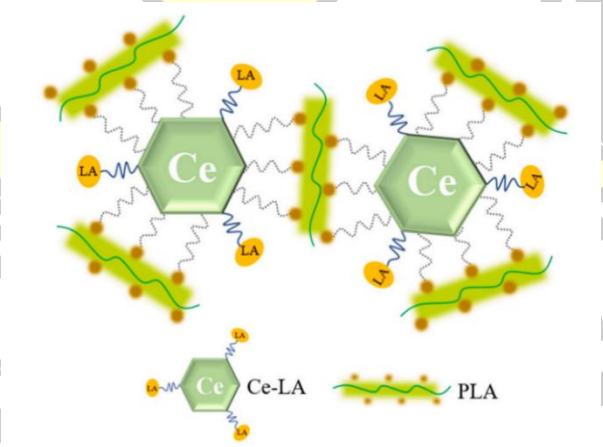


**Figure 17.** Schematic diagram of the interaction between Ce–LA and PLA [31].

When the addition of Ce–LA, it can be seen that a certain amount of Ce–LA, PLA had excellent antibacterial performance. When the amount of Ce–LA was 1.8%, the antibacterial rates of the P/CL18 film against *Staphylococcus aureus* and *Escherichia coli* were 93% and 85%, respectively, and the corresponding antibacterial performance values were 1.2 and 0.8, respectively, as shown in Table 8 [31].

**Table 8.** Comparison data of the antibacterial performance test of samples [31].

| Sample | Test strain | The mean number of viable bacteria of P/CL0 in 24 h (CFU/cm$^2$) | Mean number of viable bacteria of P/CL18 in 24 h (CFU/cm$^2$) | Antibacterial property value | Antibacterial rate (%) |
|---|---|---|---|---|---|
| P/CL18 | *Staphylococcus aureus* | $1.44\times10^4$ | $1\times10^3$ | 1.2 | 93 |
| P/CL18 | *Escherichia coil* | $2.64\times10^4$ | $3.9\times10^3$ | 0.8 | 85 |

When adding Ce–LA, the surface of PLA composites can form an antibacterial barrier. When bacteria enter the antibacterial barrier, Ce–LA begins to destroy the cell wall of bacteria and then enters the interior of bacteria to further destroy bacterial DNA and other organic physiological systems to achieve sterilization and bacteriostasis as shown in Figure 18 [31].

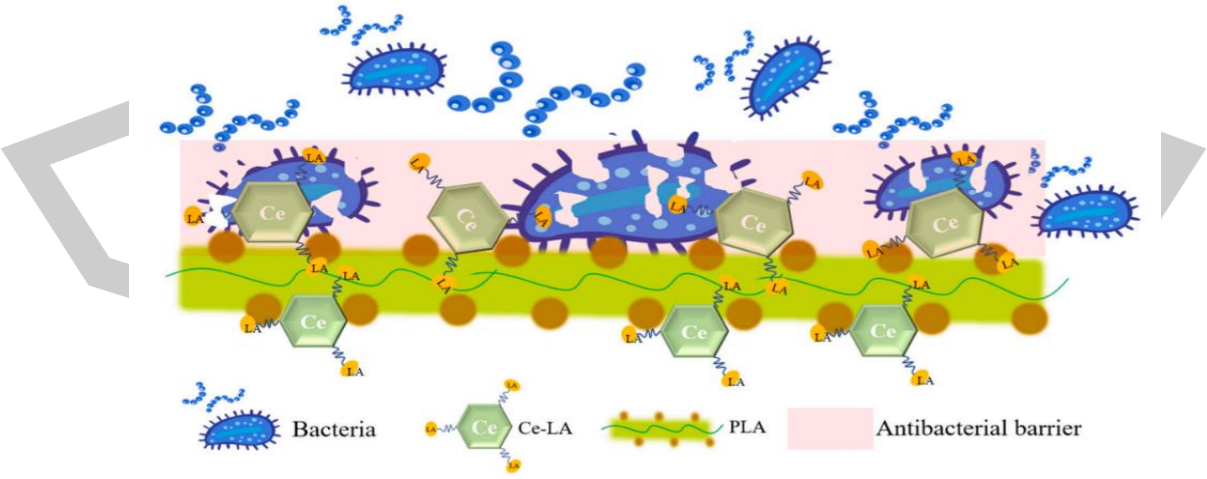


**Figure 18.** Antibacterial diagrammatic sketch of Ce–LA [31].

2.3.4 Talcum

The talcum has been used as a nucleating agent to increase the crystallinity and improve the heat resistance of the PLLA–PEG–PLLA composites. Talcum is an effective nucleating agent for developing the crystallinity content of PLLA to obtain good thermal resistant PLLA. The combination of plasticization and nucleation effects has been extensively investigated to enhance the crystallization of PLLA [24]. The PEG/talcum combination induced a faster crystallization rate and higher crystallinity content of PLLA than the PEG/clay combination. PEG acted as a plasticizer whereas talcum and clay acted as nucleating agents for this purpose. The PLLA with higher crystallinity content exhibited better thermal resistance [24].

The XRD–$X_c$ of PLLA/talcum and PLLA–PEG–PLLA/talcum composite films significantly increased with the talcum contents as summarized in Table 9. The XRD–$X_c$ of PLLA–PEG–PLLA/talcum composite films were more than the PLLA/talcum composite films for the same talcum content. This may be explained by the flexible PEG middle blocks and talcum addition having synergistic effects for the crystallization of PLLA end-blocks of PLLA–PEG–PLLA, thereby increasing their XRD–$X_c$. It has been reported that both the PEG and the talcum enhanced PLLA crystallization. PEG improved the chain mobility of PLLA, while talcum acted as a heterogeneous nucleating agent [24].

**Table 9.** XRD–$X_c$ of PLLA/talcum and PLLA-PEG-PLLA/talcum films [24].

| Composite films | Talcum (wt%) | XRD–$X_C$ (%) |
|---|---|---|
| PLLA/talcum | 0 | 0 |
| | 1 | 3.8 |
| | 2 | 6.4 |
| | 4 | 9.5 |
| | 8 | 14.7 |
| PLLA–PEG–PLLA/talcum | 0 | 12.8 |
| | 1 | 18.5 |
| | 2 | 26.6 |
| | 4 | 44.3 |
| | 8 | 51.1 |

# CHAPTER III

# RESEARCH METHODOLOGY

## 3.1 Chemicals and Equipment

### 3.1.1 Chemicals

The chemicals used in this research are listed in Table 10.

**Table 10.** Chemicals used in this research.

| Chemicals | Usage | Grade | Supplier |
|---|---|---|---|
| L-Lactic acid | Monomer precursor | Heat stable grade (L-form ≥ 97%) | PURAC (Thailand) |
| Poly(ethylene glycol) (PEG) | Initiator | Molecular weight of 20,000 g/mol | Sigma-Aldrich |
| Stannous octoate | Catalyst | 95% | Sigma |
| Joncryl® | Chain extender | ADR 4368 | BASF (Thailand) |
| Cerium (III) nitrate hexahydrate | Ce–LA precursor | 99.5% | Acros Organics |
| Sodium lactate | Ce–LA precursor | 60 wt% solution in water | Thermo Fisher Chemical |

### 3.1.2 Equipment

The equipment used in the study is shown in Table 11.

**Table 11.** Equipment used in this research.

| Equipment | Model | Company |
|---|---|---|
| $^{1}$H-NMR Spectrometer | DPX 400 | Bruker Advance |
| Gel permeation chromatograph (GPC) | GPC Waters e2695 | Alliance |
| Differential scanning calorimeter (DSC) | Pyris Diamond | PerkinElmer |
| Thermogravimetric analyzer (TGA) | SDT Q600 | TA Instruments |
| Universal testing machine (UTM) | LY-1066B | Dongguan Liyi Environmental Technology Co., Ltd. |
| X-ray diffractometer (XRD) | D8 Advance | Bruker |
| Scanning Electron Microscope (SEM) | JSM-6460LV | JEOL |
| Internal mixer | Rheomex | HAAKE |
| Vacuum oven | Vacucell | MMM Group |
| Compression molding machine | Auto CH | Carver, Inc. |

### 3.2 Synthesis of Ce-LA

$Ce(NO_3)_3$ aqueous solution (10.86 g in 25 mL) and sodium lactate aqueous solution (14.00 g in 25 mL) were mixed in a flask with a $Ce^{3+}$/lactate mole ratio of 1:3. After stirring at 35 ˚C for 4 h, ammonia was added to adjust the pH to 7, and the solution was allowed to stand for 12 h. Finally, the sediment was centrifuged and filtered and then dried at 100 ˚C in a vacuum oven for 12 h to obtain Ce–LA powder [31].

### 3.3 Synthesis of PLLA–PEG–PLLA

PLLA–PEG–PLLA with feed M.W. of 120,000 g/mol was synthesized by ring-opening polymerization in the bulk of LLA monomers under a nitrogen atmosphere at 165 ˚C for 6 h using $Sn(Oct)_2$ (0.075 mol%) as a catalyst and Joncryl ADR4368 (2 phr) as a chain extender. The PEG with M.W. of 20,000 g/mol was used as an initiator. The polymerization reaction is presented in Figure 19. The obtained PLLA–PEG–PLLA was granulated before being dried in a vacuum oven at 110 ˚C for 2 h to remove some unreacted lactides.

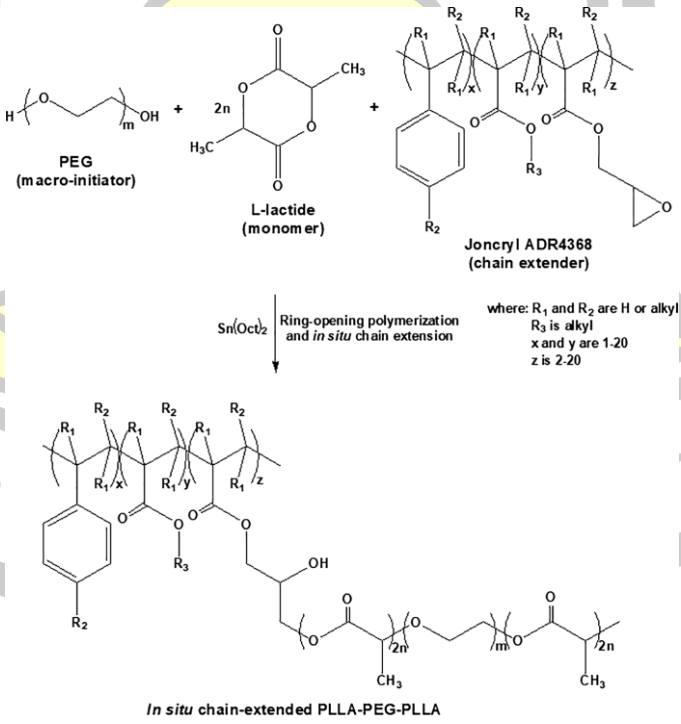


**Figure 19.** Ring-opening polymerization of a chain-extended PLLA–PEG–PLLA.

### 3.4 Preparation of PLLA-PEG-PLLA/Ce–LA composites

Before melt mixing, the samples were dried in an air flow oven at 80 ˚C for 2 h, after which the samples were melt mixed at 170˚C for 6 min in an internal mixer. After the samples were ground, they were dried in an air flow oven at 80 ˚C for 2 h. Composite films (100 × 100 × 0.2 mm) were prepared by compression molding using a hot-press machine. The samples were pre-melted at 170 ˚C for 3.0 min before being compressed with 5 tons for 2.0 min. Allowed to cool to room temperature with water flow plates under the same compression forces. The PLLA–PEG–PLLA/Ce–LA weight ratios are 100/0, 99.5/5, 99/1, 98.5/1.5, 98/2, and 75.5/2.5. Table 12 shows the formulations of the PLLA–PEG–PLLA/Ce–LA composites in this study.

**Table 12.** Formulations of PLLA–PEG–PLLA/Ce–LA film composites.

| PLLA–PEG–PLLA/Ce–LA ratio (w/w) | PLLA–PEG–PLLA (g) | Ce–LA (g) |
|---|---|---|
| 100/0 | 50 | – |
| 99.5/0.5 | 49.75 | 0.25 |
| 99/1.0 | 49.50 | 0.50 |
| 98.5/1.5 | 49.25 | 0.75 |
| 98/2.0 | 49.00 | 1.00 |
| 97.50/2.5 | 48.75 | 1.25 |

## 3.5 Characterization

Ce–LA, PLLA–PEG–PLLA, and PLLA–PEG–PLLA/Ce–LA composites were characterized by various analytical techniques as follows.

### 3.5.1 Scanning Electron Microscope (SEM)

The phase morphology of Ce–LA powder and composites was observed by SEM. The SEM was taken at 15 kV under high vacuum mode. The Ce–LA powder was sputter-coated with gold before SEM analysis. The film samples were immersed in liquid nitrogen before cryogenically fracturing. Fractured surfaces of the film samples were sputter coated with gold before SEM analysis.

### 3.5.2 Thermogravimetric analysis (TGA)

TGA was used to determine the thermal decomposition behaviors of the Ce–LA powder and composites using a thermogravimetric analyzer with a heating rate of 20 ˚C/min and a nitrogen gas flow at 100 mL/min.

### 3.5.3 X-ray diffractometry (XRD)

The crystalline structures of the Ce–LA powder and composites were determined by XRD at 25 ˚C operated at 40 kV and 40 mA CuKα radiation. For XRD, the sample was recorded in a 2θ range of 5˚to 30 ˚ at a scan rate of 3˚/min.

### 3.5.4 $^{1}$H–NMR spectroscopy ($^{1}$H-NMR)

$^{1}$H–NMR spectroscopy is a technique used to determine the chemical structure and copolymer composition of PLLA–PEG–PLLA. Deuterated chloroform ($CDCl_3$) was used as a solvent.

### 3.5.5 Gel permeation chromatography (GPC)

GPC is a technique used to analyze the molecular weight and molecular weight distribution of PLLA–PEG–PLLA. Number-average molecular weight (Mn) and dispersity index (Đ) of PLLA–PEG–PLLA were determined by GPC at 40˚C with a flow rate of 1.0 mL/min. Tetrahydrofuran was used as a solvent. Polystyrenes with narrow Đ values were used as a standard for the calibration curve.

### 3.5.6 Differential scanning calorimetry (DSC)

Thermal transition properties of Ce-LA powder, PLLA–PEG–PLLA, and composites were studied by DSC. The 5–10 mg sample was sealed in an aluminum pan that was melted at 200 ˚C for 2 min to eliminate its thermal history before quenching to 0 ˚C and re-heated from 0 to 200 ˚C at the rate of 10˚ C/min under nitrogen atmosphere to observe their glass transition temperature ($T_g$), cold crystallization temperature ($T_{cc}$), enthalpy of cold crystallization ($\Delta H_{cc}$), melting temperature ($T_m$) and enthalpy of melting ($\Delta H_m$). The degree of crystallinity from DSC ($X_c$) of PLLA–PEG–PLLA was calculated using this equation [32].

$$X_c\ (\%) = [(\Delta H_m - \Delta H_{cc})/(93.6 \times W_{PLLA})] \times 100 \qquad (2)$$

where $\Delta H_m$ and $\Delta H_{cc}$ are enthalpies of melting and cold crystallization for PLLA–PEG–PLLA. The 93.6 is the theoretical 100% $X_c$ for PLLA. $W_{PLLA}$ is a weight fraction of PLLA form $^1$H–NMR that is 0.83 for PLLA–PEG–PLLA.

### 3.5.7 Tensile Test

Tensile properties, including ultimate tensile strength, strain at break, and Young's modulus of the film samples were investigated using by tensile tester. The films (10×100 mm) were tested at 25˚C, with a speed of 50 mm/min. A gauge length of 50 mm was used. The experimental values for mechanical properties represent averages of measurements from the five replicate films.

# CHAPTER IV

# RESULTS AND DISCUSSION

## 4.1 Characterization of Ce–LA

Ce–LA was prepared from cerium (III) nitrate hexahydrate and a sodium lactate solution in water [31]. The synthesis reaction of Ce–LA is illustrated in Figure 20. In this work, the synthesized Ce–LA was calculated as a percentage of the yield as 57.6 %. Figure 21 shows an SEM image of Ce–LA powder with irregular shapes.

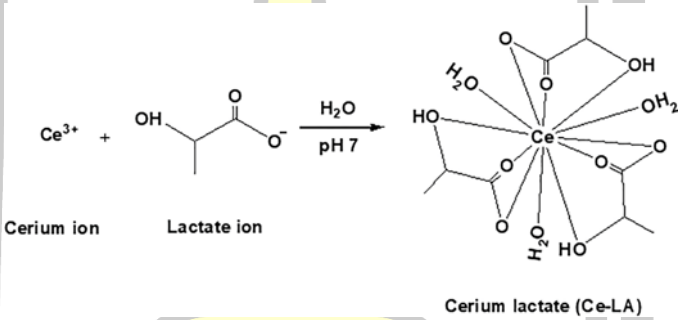


**Figure 20.** Synthesis reaction of Ce–LA.

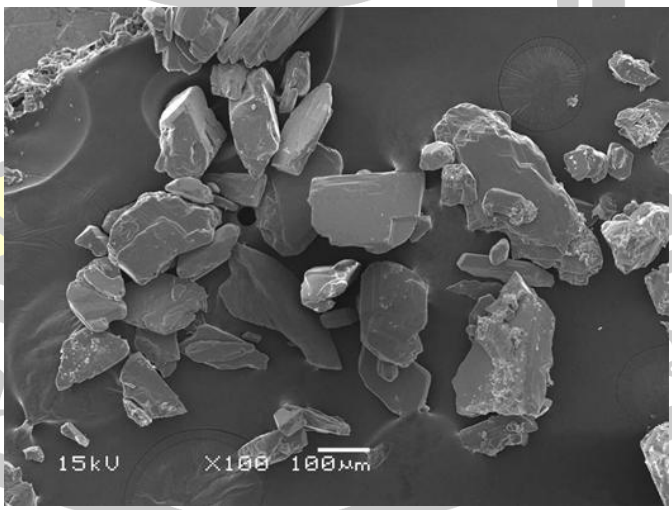


**Figure 21.** SEM micrograph of Ce–LA powder.

To determine the thermal decomposition of the Ce–LA powder, thermogravimetric (TG) and derivative TG, (DTG) thermograms were used for analysis, as shown in Figure 22. The decomposition process of Ce–LA was divided into three stages [31]. In the first stage (100–200 ˚C), the weight loss is 10 %, mainly due to the evaporation of water ligands. In the second stage (200–350 ˚C), the mass loss is 20%, which is mainly due to the breaking of the coordination bond between cerium and lactic acid. In the third stage (350–600 ˚C), the mass loss is 20%, which is the lactic acid decomposition. Char residue at 600 °C was $CeO_2$ which was 45%.

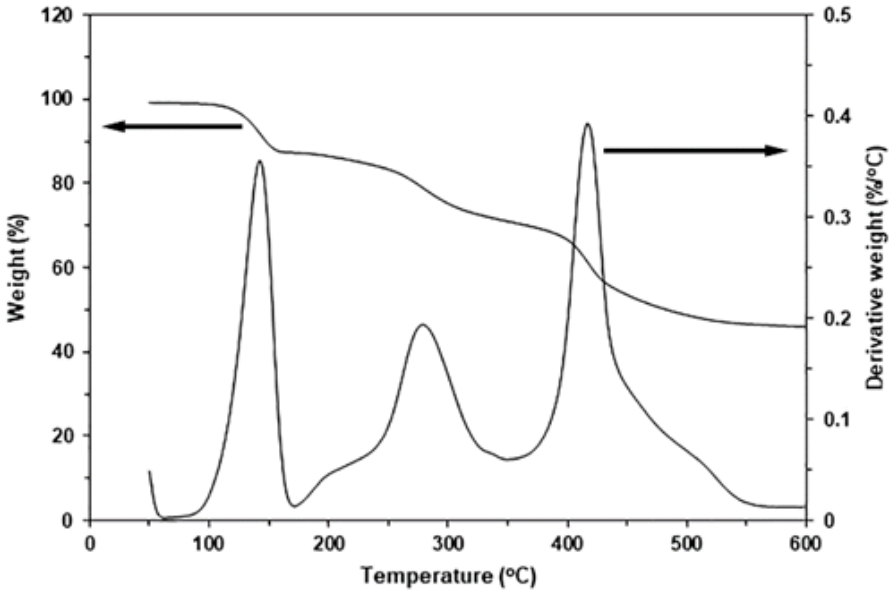


**Figure 22.** TG and DTG thermograms of Ce–LA powder.

The DSC heating and cooling thermograms of the Ce–LA had no DSC peak, as shown in Figure 23.

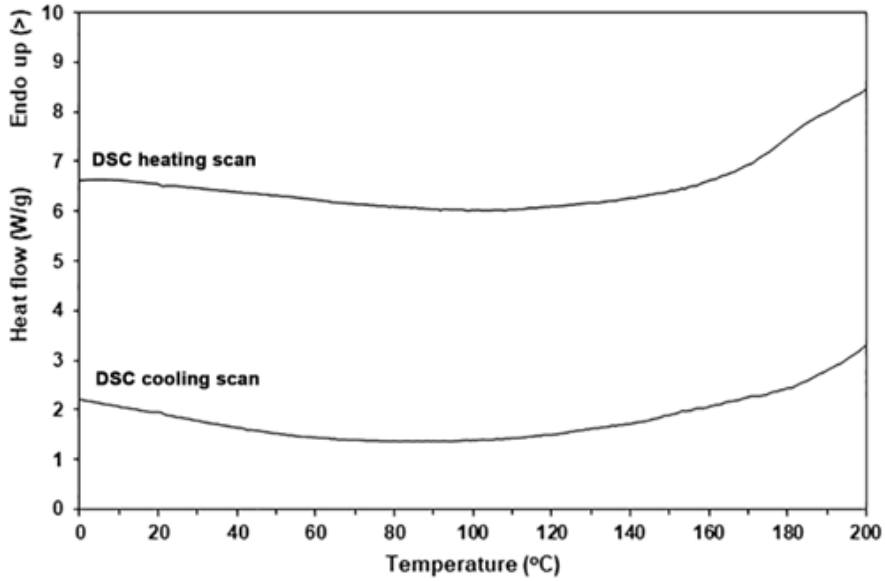


**Figure 23.** DSC heating and cooling thermograms of Ce–LA.

XRD was used to determine the crystalline structures of the synthesized Ce–LA. An XRD profile of Ce–LA exhibited diffraction peaks at 10.4˚(011), 15.2˚ (200), 17.8˚(102), and 22.2˚(212), as shown in Figure 24, attributed to Ce–LA's crystallites [31].

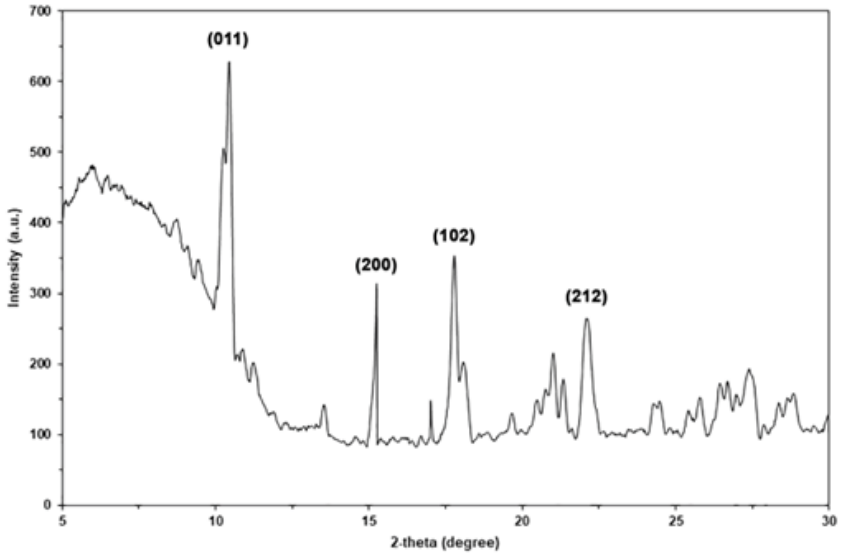


**Figure 24.** XRD profile of Ce–LA.

## 4.2 Characterization of PLLA–PEG–PLLA

### 4.2.1 Thermal transition properties

The thermal transition properties of pure PLLA–PEG–PLLA were studied using non-isothermal DSC scan. The DSC heating curve for PLLA–PEG–PLLA is presented in Figure 25, and the corresponding results are summarized in Table 13. The glass transition temperature ($T_g$) and melting temperatures ($T_m$) of PLLA–PEG–PLLA were 32 ˚C and 159 ˚C, respectively. The $T_g$ of PLLA–PEG–PLLA was lower than the pure PLLA (approximately 60 ˚C). This can be explained by flexible PEG middle blocks acting as plasticizer sites to decrease the $T_g$ of PLLA end blocks [7, 33]. The cold crystallization temperature ($T_{cc}$) and DSC-$X_c$ values of pure PLLA–PEG–PLLA were 81 ˚C and 14.2%, respectively.

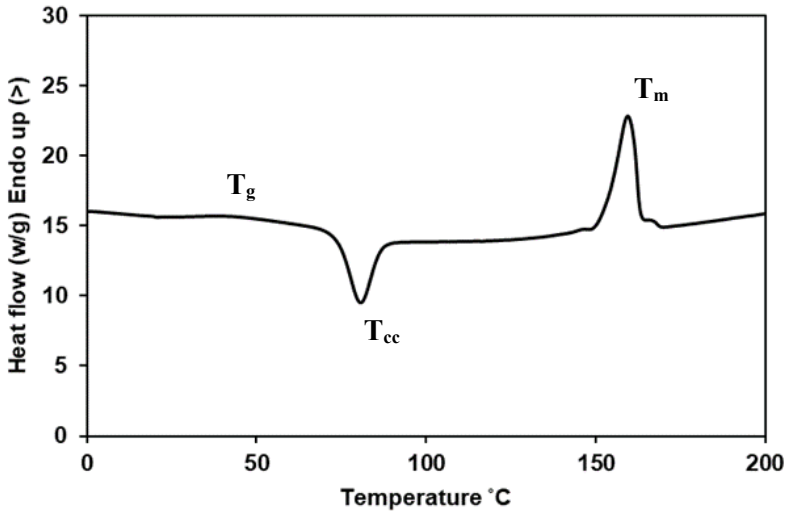


**Figure 25.** DSC heating thermogram of a chain-extended PLLA–PEG–PLLA.

**Table 13.** Thermal transition properties of PLLA–PEG–PLLA.

| Sample | $T_g$ (˚C) | $T_{cc}$ (˚C) | $\Delta H_{cc}$ (J/g) | $T_m$ (˚C) | $\Delta H_m$ (J/g) | DSC-$X_c$ (%) |
|---|---|---|---|---|---|---|
| PLLA–PEG–PLLA | 32 | 81 | 20.3 | 159 | 31.3 | 11.8 |

### 4.2.2 Thermal decomposition properties

The TG and DTG curves of PLLA–PEG–PLLA are presented in Figure 26. The decomposition process of PLLA–PEG–PLLA was divided into two stages. In the first stage (200–300 ˚C), the weight loss is 84 %, mainly due to the decomposition of PLLA end-blocks. In the second stage (300–450 ˚C), the mass loss is 16 %, which is primarily due to the decomposition of PEG middle-blocks [33,34].

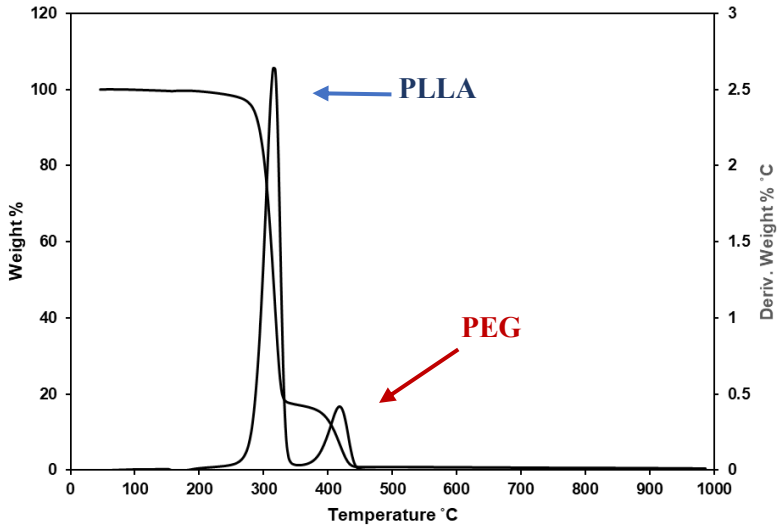


**Figure 26.** TG and DTG curves of a chain-extended PLLA–PEG–PLLA.

### 4.2.3 Chemical compositions

The chemical composition of the PLLA–PEG–PLLA was determined as LLA:ethylene oxide (LLA:EO) ratio using a $^{1}$H-NMR spectrometer at 25 ˚C, as shown in Figure 27, from methine protons of LLA units (peak 1) and methylene protons of EO units (peak 14), repeating units of PLLA and PEG blocks, respectively. The LLA:EO ratio was 60:40 mol%.

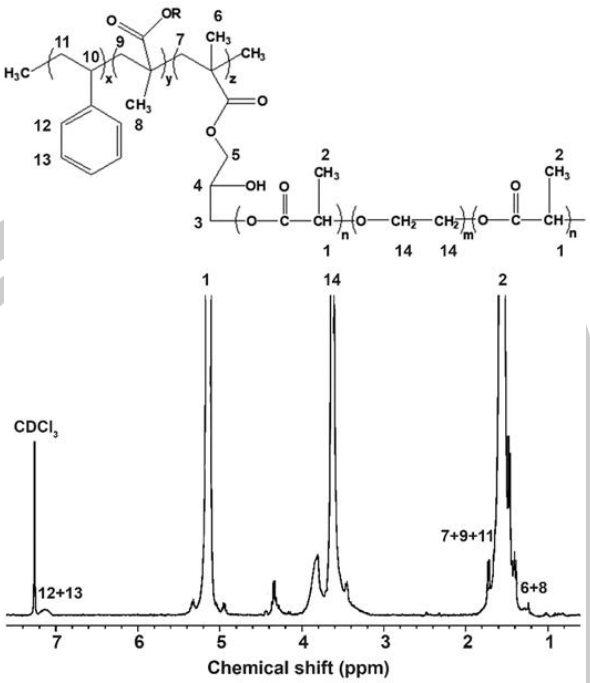


**Figure 27.** $^{1}$H-NMR spectrum of a chain-extended PLLA–PEG–PLLA.

### 4.2.4 Molecular weight characteristics

Figure 28 shows the GPC curve of PLLA–PEG–PLLA. The GPC trace of this sample exhibits an unimodal distribution. The resulting number-average molecular weight ($M_n$) and the dispersity (Đ) of the PLLA–PEG–PLLA were 108,500 g/mol and 2.2, respectively.

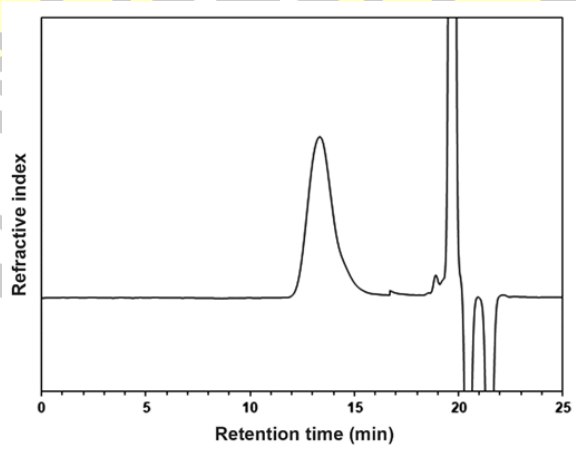


**Figure 28.** GPC curve of a chain-extended PLLA–PEG–PLLA.

### 4.3 Characterization of PLLA–PEG–PLLA/Ce–LA composite

#### 4.3.1 Thermal transition properties

The PLLA–PEG–PLLA composites with different Ce–LA contents were prepared to compare the nucleating effect of Ce–LA on the non-isothermal and isothermal DSC scans of the PLLA–PEG–PLLA matrix, as shown in Figures 29–32, respectively. In Figure 29, the $T_g$, $T_{cc}$, and $T_m$ are seen on the DSC heating thermograms. In Figure 30, the crystallization temperature ($T_c$) is seen on the DSC cooling thermograms. The DSC results of both the DSC heating and cooling scans are summarized in Table 14.

The $T_g$ and $T_m$ values of all the composites ranged from 31 to 32 ˚C and 159 to 160 ˚C, respectively, suggesting that the addition of Ce–LA did not affect both the transition of glassy-to-rubbery state and melting behavior of the PLLA–PEG–PLLA. It was found that the incorporation of Ce–LA shifted the cold crystallization temperature ($T_{cc}$) peaks from 81 ˚C to lower temperatures (75–76 ˚C), suggesting an improvement in the crystallization of polymer matrices [36–38]. Thus, this result suggests that the addition of Ce-LA enhanced the crystallization of the PLLA–PEG–PLLA matrix. Table 14 also reports the degree of crystallinity ($X_c$) values. The $X_c$ values increased from 11.8% to 15.9% with the addition of 0.5 wt% Ce-LA, which supports the idea that Ce–LA enhances the crystallizability of PLLA–PEG–PLLA by enhancing the heterogeneous nucleating effect. The $X_c$ value decreased again when the Ce–LA content was higher than the 0.5 wt%. This may be due to the aggregation of the inorganic fillers at higher loading in the polymeric matrix, suppressing its nucleation effectiveness [25,39]. However, the $X_c$ values of all the composites in the range of 13.7–15.9% were still higher than that of the pure PLLA–PEG–PLLA (11.8%).

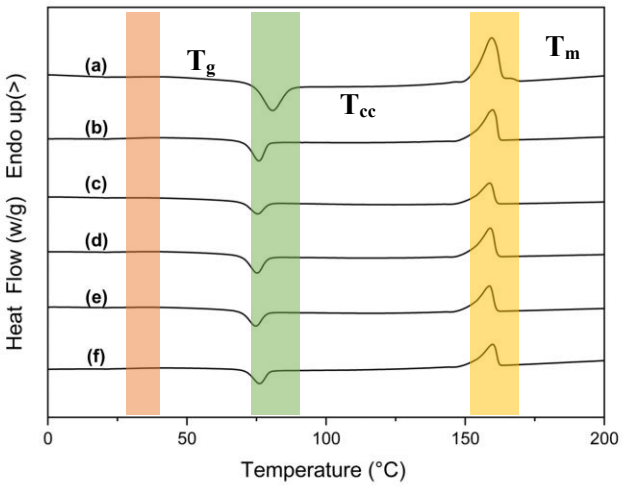


**Figure 29.** DSC heating thermograms of PLLA–PEG–PLLA composites (a) without Ce–LA and with Ce–LA contents of (b) 0.5%, (c) 1%, (d) 1.5%, (e) 2%, and (f) 2.5%.

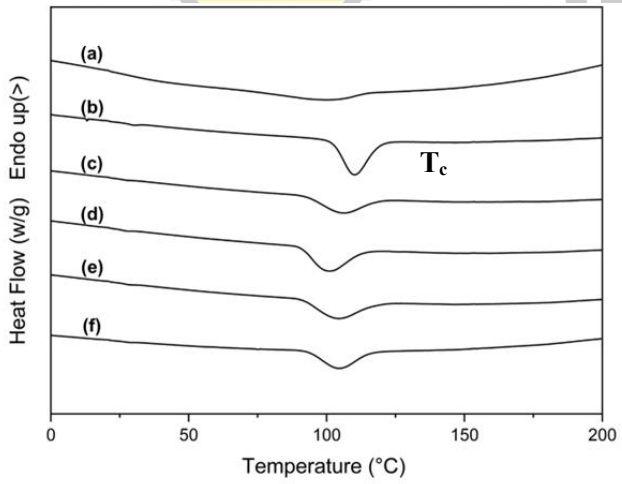


**Figure 30.** DSC cooling thermograms of PLLA–PEG–PLLA composites (a) without Ce–LA and with Ce–LA contents of (b) 0.5%, (c) 1%, (d) 1.5%, (e) 2%, and (f) 2.5%.

**Table 14.** Thermal transition properties of PLLA-PEG-PLLA/Ce-LA composites from DSC heating thermograms.

| Ce–LA (wt%) | $T_g$ (˚C) | $T_{cc}$ (˚C) | $\Delta H_{cc}$ (J/g) | $T_m$ (˚C) | $\Delta H_m$ (J/g) | $X_c$ (%) |
|---|---|---|---|---|---|---|
| – | 32 | 81 | 20.3 | 159 | 31.3 | 11.8 |
| 0.5 | 31 | 75 | 17.6 | 160 | 32.4 | 15.9 |
| 1 | 32 | 75 | 16.0 | 160 | 29.7 | 14.8 |
| 1.5 | 32 | 75 | 17.4 | 159 | 30.6 | 14.3 |
| 2 | 31 | 75 | 17.8 | 159 | 30.6 | 14.1 |
| 2.5 | 31 | 76 | 17.5 | 160 | 31.1 | 13.7 |

In Figures 31, exothermic peaks of crystallization temperature ($T_c$) were detected, and Table 15 provides the $T_c$ values. The $T_c$ peak of the pure PLLA–PEG–PLLA (99 ˚C) shifted to a higher temperature (110 ˚C) with the incorporation of 0.5 wt% Ce–LA, enhancing crystallization of the PLLA–PEG–PLLA. The crystallization rate of the PLLA–PEG–PLLA matrix was accelerated by the heterogeneous nucleating agents, as indicated by the $T_c$ peak shifting to a higher temperature during the DSC cooling scan [36, 40–42]. The $T_c$ peak shifted to a lower temperature again when the Ce–LA content was over 0.5 wt%. However, the $T_c$ values of all the composites (102–110 ˚C) were still higher than that of the pure PLLA–PEG–PLLA. In addition, the enthalpy of crystallization ($\Delta H_c$) increased with the addition of Ce–LA suggesting that the Ce–LA accelerated the crystallization of PLLA blocks during a cooling scan.

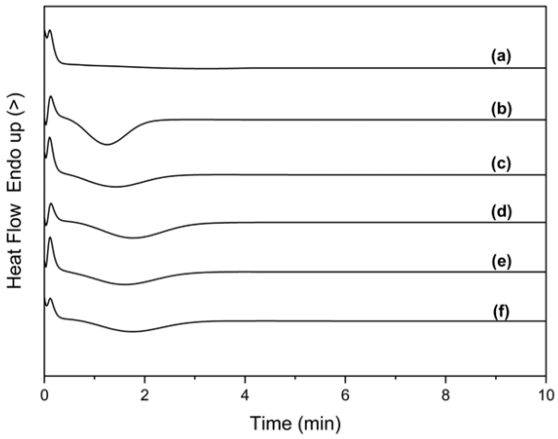


**Figure 31.** Isothermal crystallization curves at 120 ˚C of PLLA–PEG–PLLA composites (a) without Ce–LA and with Ce–LA contents of (b) 0.5%, (c) 1%, (d) 1.5%, (e) 2%, and (f) 2.5%.

**Table 15.** Thermal transition properties of PLLA-PEG-PLLA/Ce-LA composites from DSC cooling thermograms.

| Ce–LA (wt%) | $T_c$ (˚C) | $\Delta H_c$ (J/g) |
|---|---|---|
| 0 | 99 | 13.3 |
| 0.5 | 110 | 31.7 |
| 1 | 106 | 30.2 |
| 1.5 | 102 | 29.6 |
| 2 | 103 | 31.2 |
| 2.5 | 103 | 31.0 |

Additionally, we examined the crystallization characteristics of the composites using the half-time of crystallization ($t_{1/2}$), which was obtained from Figure 31. The polymer samples exhibited a relative crystallinity of 50% during isothermal scans at $t_{1/2}$, as shown in Figure 32. The obtained $t_{1/2}$ values are reported in Table 16. The $t_{1/2}$ values decreased from 3.4 min to 1.3 min with the addition of 0.5 wt% Ce–LA, which confirmed that the PLLA–PEG–PLLA matrix was heterogeneously nucleated by the Ce–LA. The $t_{1/2}$ value increased again when the Ce–LA content was higher than 0.5 wt%. Aggregation of Ce–LA particles may reduce nucleation effectiveness. However,

the $t_{1/2}$ values of all the composites (1.3–1.8 min) were still faster than that of the pure PLLA–PEG–PLLA (3.4 min), indicating that all the composites had a faster crystallization rate than that of the pure PLLA–PEG–PLLA. The following Avrami Equation (3) was employed to analyze the crystallization kinetics of composite materials through the Avrami exponent ($n$) and the crystallization rate constant ($k$) [43, 44].

$$1 - X_t = \exp(-kt^n) \quad (3)$$

where $X_t$ is the relative crystallinity as a function of time, $t$ is the crystallization time, $n$ is the Avrami exponent, and $k$ is the crystallization rate constant.

The $n$ and $k$ values obtained from $\log[-\ln(1-X_t)$ versus $\log(t)$ graphs are also summa rized in Table 16. All $R^2$ values exceeded 0.99, indicating that the graphs exhibited excellent linear regression. The pure PLLA–PEG–PLLA had higher $n$ and lower $k$ values compared to the composites, indicating that it has the slowest crystallization rate [44, 45]. The composite containing 0.5 wt% Ce–LA had a lower $n$ value and higher $k$ value compared to the pure PLLA–PEG–PLLA, suggesting that added Ce–LA accelerated the PLLA–PEG–PLLA crystallization. This may be explained by the $n$ value increased and the $k$ value decreased when the Ce–LA content was over 0.5 wt%. The aggregation of Ce–LA may have reduced nucleation efficiency. The results will be confirmed later using SEM analysis. However, the $n$ values of all the composites (3.3191–3.5364) were still lower and the $k$ values were still higher (0.0862–0.3590 $min^{-1}$) than those of the pure PLLA–PEG–PLLA ($n$ = 3.5916 and $k$ = 0.0086 $min^{-1}$). This confirmed that all the composites had a faster crystallization rate than that of the pure PLLA–PEG–PLLA. All the $n$ values exceeded 2.0, indicating a heterogeneous nucleating effect [46]. It is clear from the DSC results that Ce–LA is a good nucleating agent for PLLA–PEG–PLLA.

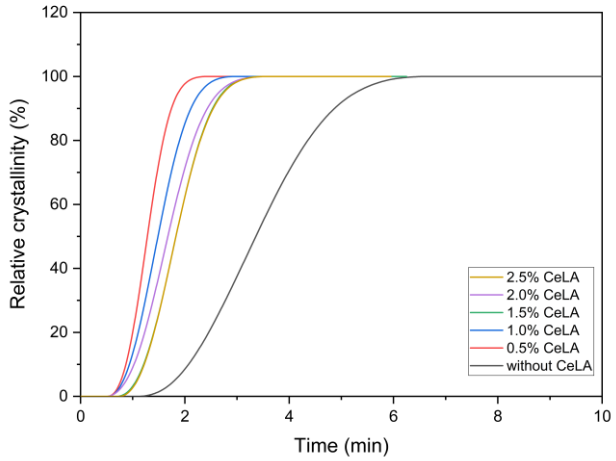


**Figure 32.** Relative crystallinity as a function of time curves of PLLA–PEG–PLLA composites.

**Table 16.** Half–time of crystallization ($t_{1/2}$) and Avrami parameters (n and K) of PLLA–PEG–PLLA composites.

| **Ce–LA content (wt%)** | **$t_{1/2}$ (min)** | ***n*** | ***K*** **($min^{-1}$)** | ***$R^2$*** |
|---|---|---|---|---|
| - | 3.4 | 3.5916 | 0.0086 | 0.9962 |
| 0.5 | 1.3 | 3.3191 | 0.3590 | 0.9999 |
| 1 | 1.5 | 3.4340 | 0.1786 | 0.9997 |
| 1.5 | 1.8 | 3.5364 | 0.0862 | 0.9999 |
| 2 | 1.7 | 3.4335 | 0.1152 | 0.9988 |
| 2.5 | 1.8 | 3.4388 | 0.0919 | 0.9999 |

### 4.3.2 Crystalline structures

X-ray diffraction was used to evaluate the crystalline structures of the samples. As shown in Figure 33, the pure PLLA–PEG–PLLA exhibited a broad diffraction peak at 16.9˚ (200)/(110), which is attributed to the crystallites of the PLLA blocks [42,47,48]. All the composites also exhibited an XRD peak at 16.9˚ corresponding to the α crystalline phase with an orthorhombic unit cell of PLLA [49,50], indicating that the addition of Ce-LA did not change the crystalline structure of the PLLA–PEG–PLLA matrix. An XRD profile of Ce–LA exhibited diffraction peaks at 10.4˚ (011), 15.2˚ (200), 17.8˚ (102), and 22.2˚ (212), as shown in Figure 24. The XRD profiles of the composites had no XRD peaks of Ce-LA. This may be because they were overlapped by the amorphous halo of the PLLA–PEG–PLLA matrix. It can be clearly seen that the peak intensity at 16.9˚ increased when the 0.5 wt% Ce–LA was included, suggesting that the PLLA–PEG–PLLA crystallinity increased. This supports the idea that Ce–LA enhances the nucleating effect. However, the peak intensity decreased again when the Ce–LA content exceeded 0.5 wt%. This may be explained by the Ce–LA being aggregated when the amount of Ce–LA was higher than 0.5 wt%, decreasing its nucleation effectiveness, as described in the later SEM analysis.

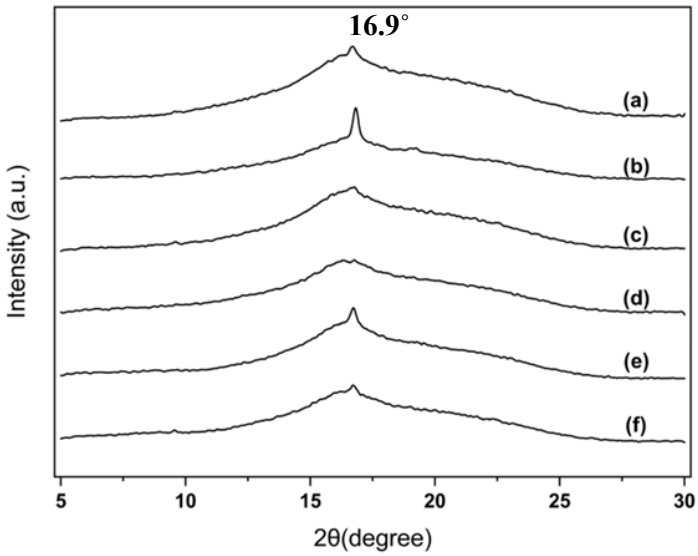


**Figure 33.** XRD patterns of PLLA–PEG–PLLA /Ce–LA composites (a) without Ce–LA and with Ce–LA contents of (b) 0.5%, (c) 1%, (d) 1.5%, (e) 2%, and (f) 2.5%.

### 4.3.3 Phase morphology

Figure 34 illustrates the SEM micrographs of film cross-sections of the film samples. The film cross-section of the pure PLLA–PEG–PLLA exhibited rough surfaces due to its high flexibility. Additionally, we observed the presence of tiny needles on the film cross-section. The high flexibility of the PLLA–PEG–PLLA matrix may have caused it to stretch prior to film fracture. All the composite films also have tiny needles on film cross-sections, indicating that they are flexible.

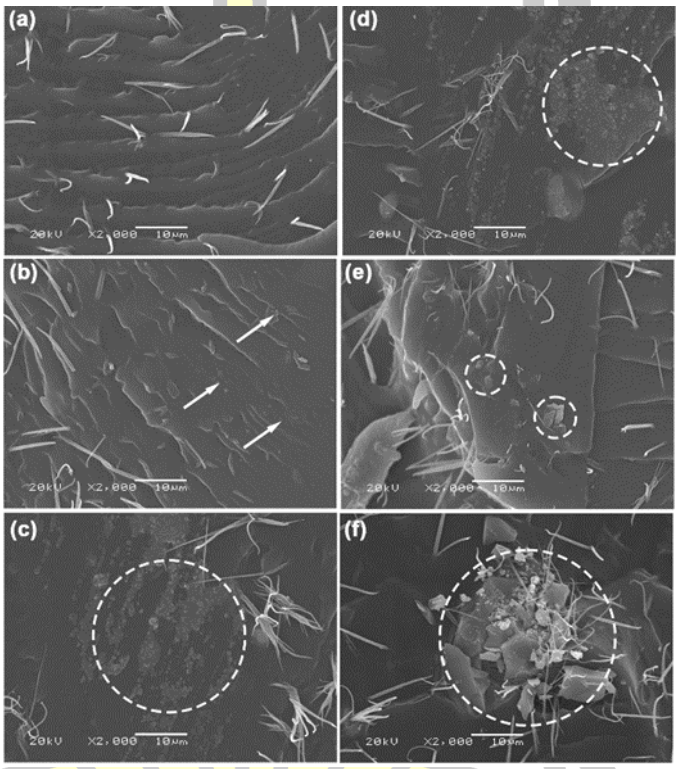


**Figure 34.** SEM micrographs of film cross-sections of PLLA–PEG–PLLA/Ce–LA composite films (some Ce–LA particles were labeled by white arrows, and some Ce–LA aggregates were labeled by white circles).

The Ce–LA particles were well distributed on the film matrix for 0.5 wt% Ce–LA. However, aggregation of small Ce–LA particles was observed when the Ce–LA content was over 0.5 wt%. This may be due to the difference in hydrophilicity between the polymer matrix and the inorganic fillers [50–53]. The composites contained smaller Ce–LA particles than the originals (see Figure 21). This may be due

to the breakdown of Ce– LA particles during the melt-mixing process. The SEM results could explain the decrease in nucleation effectiveness of Ce–LA as its content increased beyond 0.5 wt%, as described in the above DSC and XRD analyses. Aggregation of large Ce– LA particles was found for the 2.0 and 2.5 wt% Ce– LA composites. The high Ce– LA content made particles difficult to break during the melt-mixing process. However, good wettability between the PLLA–PEG–PLLA matrix and the Ce– LA was found. The Ce– LA particles did not fall out from the PLLA–PEG–PLLA matrix during cryofracture.

### 4.3.4 Thermal decomposition properties

The TG and DTG thermograms in Figures 35(a) and 35(b), respectively were used to investigate thermal decomposition characteristics. Table 17 summarizes the TG and DTG results. As shown in Figure 35(a), the pure PLLA–PEG–PLLA thermally decomposed in two steps at different temperatures: PLLA blocks decomposed first, at 250–350˚C, and PEG blocks decomposed at 350–450˚C [34,35]. The thermal decomposition ranges of the PLLA blocks shifted to higher temperatures with the incorporation of Ce–LA, but those of the PEG blocks did not shift, showing that adding Ce–LA improved the PLLA block's thermal stability.

As shown in Table 17, the residue weights of the composites at 600˚C (0.75–2.12%) were higher than that of the pure PLLA–PEG–PLLA (0.39%) and consistently increased with Ce–LA content. This is because Ce–LA has a high residue weight at 600˚C (45%), as shown in Figure 22.

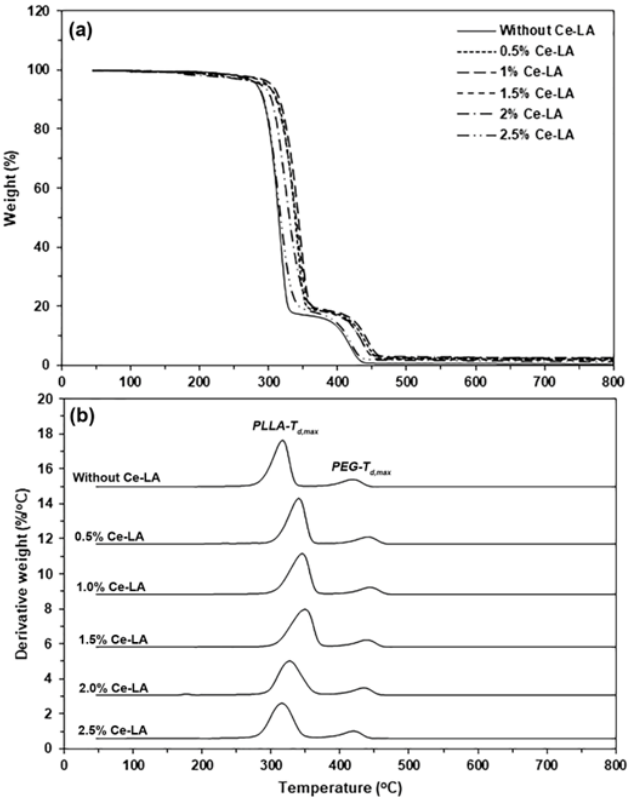


**Figure 35.** (a) TG and (b) DTG thermograms of PLLA–PEG–PLLA/Ce–LA composites.

**Table 17.** TG and DTG results of PLLA–PEG–PLLA/Ce–LA composites.

| Ce–LA content (wt%) | Residue Weight at 600 ˚C (%) [a] | PLLA-$T_{d,max}$ (˚C) [b] | PEG-$T_{d,max}$ (˚C) [b] |
|---|---|---|---|
| - | 0.39 | 310 | 418 |
| 0.5 | 0.75 | 316 | 417 |
| 1 | 1.06 | 319 | 419 |
| 1.5 | 1.47 | 327 | 417 |
| 2 | 1.88 | 313 | 418 |
| 2.5 | 2.12 | 311 | 417 |

[a] Obtained from Figure 35(a).

[b] Obtained from Figure 35(b).

The temperature at maximum decomposition rate ($T_{d,max}$) peaks of the PLLA blocks (PLLA-$T_{d,max}$) and the PEG blocks (PEG-$T_{d,max}$) were detected in the DTG thermograms, as shown in Figure 35(b). Table 17 summarizes these $T_{d,max}$ values. The pure PLLA–PEG–PLLA had the PLLA $T_{d,\,max,}$ and PEG-$T_{d,max}$ peaks at 310 ˚C and 418 ˚C, respectively, while the composites had PLLA-$T_{d,max}$ values between 311 ˚C and 327 ˚C, supporting the idea that the incorporation of Ce–LA improved the PLLA block's thermal stability. The PLLA-$T_{d,max}$ value increased with Ce-LA content until 1.5 wt%. This may be due to the large Ce–LA particles being aggregated when the Ce–LA content was higher than 1.5 wt%, as described in the above SEM analysis. The PLLA-$T_{d,max}$ value then decreased again when the Ce–LA content exceeded 1.5 wt%. The PEG-$T_{d,max}$ values of composites (417–419 ˚C) were nearly equal to that of the pure triblock copolymer (418 ˚C). According to the report, the incorporation of Ce–LA reduced the intermolecular forces between the PLLA chains, thereby decreasing the PLLA's thermal stability [31]. Surprisingly, this work found that the added Ce–LA enhanced the thermal stability of the PLLA blocks. We have reported that blending PLLA–PEG–PLLA with inorganic fillers, such as calcium carbonate ($CaCO_3$) [25] and zinc phenylphosphate (PPZn) [57], improved the PLLA block's thermal stability. The thermal stability of the triblock copolymer matrix was improved by $CaCO_3$, but the PLLA matrix did not experience any improvement. Therefore, the improved phase compatibility between the PLLA blocks and Ce–LA, facilitated by the PEG blocks, may explain the enhanced heat transfer between them and the resulting increase in thermal stability.

**4.3.5 Tensile properties**

Figure 36 displays the tensile curves of the sample films, while Table 18 summarizes the results of the tensile test. According to the above SEM analysis, the tensile curve of the pure PLLA–PEG–PLLA showed a yield point, suggesting that it had high flexibility. The incorporation of Ce–LA increased both the tensile strength and Young's modulus of films until the Ce–LA content was 1.5 wt%. The ultimate tensile strength of the composite film increased by 36%, and the Young's modulus increased by 53% when 1.5% Ce–LA was incorporated, compared to the pure PLLA–

PEG–PLLA film. The PLLA–PEG–PLLA mechanical properties were improved by the Ce–LA particles' fine dispersion within the matrix [38,53,55]. These tensile values decreased again when the Ce–LA content was over 1.5 wt%. This may be explained by the decrease in the reinforcing effectiveness of Ce–LA, which could occur from the aggregation of large Ce–LA particles, as detailed in the above SEM results, which reduce stress transfer between polymer matrices and filler particles [56,57].

All the composites exhibited ultimate tensile strength and Young's modulus values were greater than the pure PLLA–PEG–PLLA. This suggests that Ce–LA enhanced the reinforcing effect for the PLLA–PEG–PLLA. Additionally, adding Ce–LA to increase the crystallinity of the PLLA–PEG–PLLA (see Table 14) likely also enhanced the ultimate tensile strength and Young's modulus of the film samples. This is because the crystallites of the PLLA–PEG–PLLA matrix acted as physical cross-linked sites. As the Ce–LA content increased, the strain at break in the composites steadily decreased. It is well known that the incorporation of inorganic fillers decreases the flexibility of polymeric matrices because the rigid fillers restrict the ductile flow of polymer chains [52,58]. All the composites showed a yield point, confirming the above SEM analysis's conclusion that all the composites remained flexible.

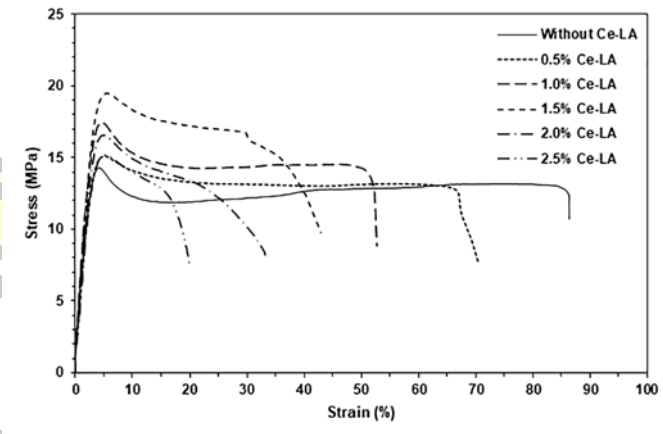


**Figure 36.** Tensile curves of PLLA–PEG–PLLA/Ce–LA composites.

**Table 18.** Tensile properties of PLLA–PEG–PLLA/Ce–LA composites.

| Ce–LA content (wt%) | Ultimate tensile strength (MPa) | Strain at break (%) | Young's modulus (MPa) |
|---|---|---|---|
| - | 14.3 ± 0.6 | 86.3 ± 2.4 | 204 ± 18 |
| 0.5 | 15.1 ± 0.4 | 70.5 ± 5.1 | 230 ± 20 |
| 1 | 17.4 ± 0.6 | 52.6 ± 6.5 | 258 ± 15 |
| 1.5 | 19.5 ± 0.5 | 42.9 ± 5.2 | 312 ± 21 |
| 2 | 16.6 ± 0.3 | 33.2 ± 4.7 | 262 ± 24 |
| 2.5 | 15.2 ± 0.4 | 19.9 ± 6.8 | 254 ± 14 |

# CHAPTER V

# CONCLUSIONS

Most of the results presented in the preceding Chapter 4 have already been discussed in detail. The final Chapter 5 of this thesis now aims to bring together the main conclusions and correlate them as far as possible. These conclusions can be divided under the following main headings.

- Synthesis and characterization of Ce–LA
- Synthesis and characterization of PLLA–PEG–PLLA
- Preparation and characterization of PLLA–PEG–PLLA/Ce–LA composites

## 5.1 Synthesis and characterization of Ce–LA

Ce–LA was successfully synthesized from $Ce(NO_3)_3$ and sodium lactate. Its % yield was about 57.6%. The resulting Ce–LA was irregular shapes as observed from SEM analysis. The thermal decomposition of Ce–LA contained three stages as determined from TGA technique. The XRD profile of Ce–LA confirmed the crystalline structure of Ce–LA crystal.

## 5.2 Synthesis and characterization of PLLA–PEG–PLLA

PLLA–PEG–PLLA with feed M.W. of 120,000 g/mol was synthesized by ring-opening polymerization in the bulk of LLA monomer under a nitrogen atmosphere at 165 ˚C for 6 h using $Sn(Oct)_2$ as a catalyst and Joncryl ADR4368 as a chain extender. The PEG with M.W. of 20,000 g/mol was used as an initiator.

The PLLA–PEG–PLLA characterization in this work was characterized using a combination of analytical techniques, specifically: thermal analysis (DSC and TG), spectroscopic analysis ($^1$H-NMR), and molecular weight measurement (GPC). The main conclusions arising from the results obtained (Chapter 4) can be summarized as follows: The results indicated from DSC, the PLLA–PEG–PLLA exhibited lower $T_g$

(32 ˚C) than the PLLA (~60 ˚C). From TGA, the decomposition process of PLLA-PEG-PLLA was divided into two stages. In the first stage (200-300 ˚C), the weight loss is 84 %, mainly due to the decomposition of PLLA end-blocks. In the second stage (300-450 ˚C), the mass loss is 16 %, which is primarily due to the decomposition of PEG middle-blocks, From $^{1}$H-NMR, the chemical functional groups of The PLLA–PEG–PLLA was indicated. Moreover, chemical bonding between the PEG middle-blocks and polylactide end-blocks was confirmed. From GPC curves, the GPC traces of these samples exhibit an unimodal distribution. Its number-average molecular weight ($M_n$) was 108,500 and dispersity (Đ) was 2.2.

**5.3 Preparation and characterization of PLLA–PEG–PLLA/Ce–LA composite**

The PLLA–PEG–PLLA/Ce–LA composites were prepare by melt mixing. The Ce–LA contents of 0, 0.5, 1.0, 1.5, 2.0, and 2.5 wt% were investigated. The PLLA–PEG–PLLA/Ce–LA composite characterization in this work was characterized using a combination of analytical techniques, specifically: thermal analysis (DSC, TG), crystalline structures (XRD), phase morphology (SEM), and tensile properties. The main conclusions arising from the results obtained (Chapter 4) can be summarized as follows: The results indicated that the 0.5 wt% Ce–LA exhibited the best nucleation efficiency for the PLLA–PEG–PLLA matrix. The highest $X_c$, the highest $T_c$, and the lowest $t_{1/2}$ values of the composites were obtained from DSC analysis when 0.5 wt% Ce–LA was incorporated. The 1.5 wt% Ce–LA composite had the best thermal stability and tensile properties of the composites. The highest PLLA-$T_{d,max}$ and the highest tensile strength values of the composites were obtained from TGA and tensile analyses, respectively, when the Ce–LA content was 1.5 wt%.

# REFERENCES

1. Vroman, I., & Tighzert, L. (2009). Biodegradable polymers. *Materials*, *2*(2), 307-344.
2. Samir, A., Ashour, F. H., Hakim, A. A., & Bassyouni, M. (2022). Recent advances in biodegradable polymers for sustainable applications. *Npj Materials Degradation*, *6*(1), 68.
3. Pohanka, M. (2020). D–lactic acid as a metabolite: toxicology, diagnosis, and detection. *BioMed Research International*, *2020*(1), 3419034.
4. Saeidlou, S., Huneault, M. A., Li, H., & Park, C. B. (2012). Poly(lactic acid) crystallization. *Progress in Polymer Science*, *37*(12), 1657-1677.
5. Wee, Y., Kim, J., & Ryu, H. (2006). Biotechnological Production of Lactic Acid and Its Recent Applications. *Food Technology and Biotechnology*, 44(2) 163–172.
6. Moon, S. I., Lee, C. W., Miyamoto, M., & Kimura, Y. (2000). Melt polycondensation of L-lactic acid with Sn (II) catalysts activated by various proton acids: A direct manufacturing route to high molecular weight Poly (L-lactic acid). *Journal of Polymer Science Part A: Polymer Chemistry*, *38*(9), 1673–1679.
7. Baimark, Y., Rungseesantivanon, W., & Prakymoramas, N. (2020). Synthesis of flexible poly(L-lactide)-*b*-polyethylene glycol-*b*-poly(L-lactide) bioplastics by ring-opening polymerization in the presence of chain extender. *e-Polymers*, *20*(1), 423–429.
8. Martin, O., & Avérous, L. (2001). Poly(lactic acid): Plasticization and properties of biodegradable multiphase systems. *Polymer*, *42*(14), 6209–6219.
9. Du, H., Sun, X., Chong, X., Yang, M., Zhu, Z., & Wen, Y. (2023). A review on smart active packaging systems for food preservation: Applications and future trends. *Trends in Food Science & Technology*, 141, 104200.
10. Caleb, O. J., & Belay, Z. A. (2023). Role of biotechnology in the advancement of biodegradable polymers and functionalized additives for food packaging systems. *Current Opinion in Biotechnology,* 83, 102972.
11. Bikiaris, N. D., Klonos, P. A., Kyritsis, A., & Barmpalexis, P. (2024). Structural and thermodynamical investigation in triblock copolymers of polylactide and poly (ethylene glycol), PLA-*b*-PEG-*b*-PLA, envisaged for medical applications. *Materials Today Communications,* 38, 107799.
12. Pan, P., Yang, J., Shan, G., Bao, Y., Weng, Z., Cao, A., Yazawa, Y., & Inoue, Y. (2012). Temperature-variable FTIR and solid-state $^{13}C$ NMR investigations on crystalline structure and molecular dynamics of polymorphic poly(L-lactide) and poly(L-lactide)/poly(D-lactide) stereocomplex. *Macromolecules*, *45*(1), 189–197.
13. Perego, G., Cella, G. D., & Bastioli, C. (1996). Effect of molecular weight and crystallinity on poly (lactic acid) mechanical properties. *Journal of Applied Polymer Science*, *59*(1), 37–43.
14. Li, Y., & Shimizu, H. (2009). Improvement in toughness of poly(l–lactide) (PLLA) through reactive blending with acrylonitrile–butadiene–styrene

copolymer (ABS): Morphology and properties. *European Polymer Journal*, *45*(3), 738–746.

15. Zhang, H., Wang, G., & Yang, H. (2011). Drug delivery systems for differential release in combination therapy. *Expert opinion on drug delivery*, *8*(2), 171–190.
16. Ding, Y., Feng, W., Lu, B., Wang, P., Wang, G., & Ji, J. (2018). PLA–PEG–PLA tri-block copolymers: Effective compatibilizers for promotion of the interfacial structure and mechanical properties of PLA/PBAT blends. *Polymer*, *146*, 179–187.
17. Breche, Q., Chagnon, G., Machado, G., Girard, E., Nottelet, B., Garric, X., & Favier, D. (2016). Mechanical behavior's evolution of a PLA–*b*–PEG–*b*–PLA triblock copolymer during hydrolytic degradation. *Journal of the mechanical behavior of biomedical materials*, 60, 288–300.
18. Ruan, G., & Feng, S. S. (2003). Preparation and characterization of poly (lactic acid)–poly (ethylene glycol)–poly (lactic acid) (PLA–PEG–PLA) microspheres for controlled release of paclitaxel. *Biomaterials*, 24(27), 5037–5044.
19. Shin, H., Thanakkasaranee, S., Sadeghi, K., & Seo, J. (2022). Preparation and characterization of ductile PLA/PEG blend films for eco-friendly flexible packaging application. *Food Packaging and Shelf Life*, 34, 100966.
20. Baimark, Y., Rungseesantivanon, W., & Prakymoramas, N. (2018). Improvement in melt flow property and flexibility of poly(L–lactide)–*b*–poly(ethylene glycol)–*b*–poly(L–lactide) by chain extension reaction for potential use as flexible bioplastics. *Materials & Design*, 154, 73–80.
21. Jirum, J & Baimark,Y. (2021). Thermal and mechanical properties of flexible poly(L–lactide)–*b*–polyethylene glycol–*b*–poly(L–lactide)/microcrystalline cellulose biocomposites. *Asian Journal of Chemistry,* 33(9), 2135–2142
22. Phromsopha, T & Baimark, Y. (2022). Improvement in mechanical properties of flexible poly(L–lactide)–*b*–polyethylene glycol–*b*–(L–lactide) bioplastic by melt blending with boron nitride. *GEOMATE Journal*, *23*(96), 19–24.
23. Phromsopha, T & Baimark, Y. (2023). Synthesis of Poly(L–lactide)–*b*–poly(ethylene glycol)–*b*–poly(L–lactide) bioplastic with bio-based isosorbide diester. *Asian Journal of Chemistry,* 35(7), 1625–1631
24. Srisuwan, Y., & Baimark, Y. (2022). Synergistic effects of PEG middle-blocks and talcum on crystallizability and thermomechanical properties of flexible PLLA–*b*–PEG–*b*–PLLA bioplastic. *e–Polymers*, *22*(1), 389–398.
25. Srihanam, P., Thongsomboon, W., & Baimark, Y. (2023). Phase morphology, mechanical, and thermal properties of calcium carbonate-reinforced poly(L–lactide)–*b*–poly(ethylene glycol)–*b*–poly(L–lactide) bioplastics. *Polymer*, 15, 301.
26. Tábi, T., Ageyeva, T., & Kovács, J. G. (2022). The influence of nucleating agents, plasticizers, and molding conditions on the properties of injection molded PLA products. *Materials Today Communications,* 32, 103936.

27. Yang, T. C., Hung, K. C., Wu, T. L., Wu, T. M., & Wu, J. H. (2015). A comparison of annealing process and nucleating agent (zinc phenylphosphonate) on the crystallization, viscoelasticity, and creep behavior of compression–molded poly (lactic acid) blends. *Polymer Degradation and Stability*, *121*, 230–237.
28. Yang, J. Y., Kim, D. K., Han, W., Park, J. Y., Kim, K. W., & Kim, B. J. (2022). Effect of nucleating agents addition on thermal and mechanical properties of natural fiber-reinforced polylactic acid composites. *Polymers*, *14*(20), 4263.
29. Deghiche, A., Haddaoui, N., Zerriouh, A., Fenni, S. E., Cavallo, D., Erto, A., & Benguerba, Y. (2021). Effect of the stearic acid-modified $TiO_2$ on PLA nanocomposites: Morphological and thermal properties at the microscopic scale. *Journal of Environmental Chemical Engineering*, *9*(6), 106541.
30. Jacoby, P. (2021). Nucleating Agents & Clarifiers Selection Tips for Polypropylene. Retrieved January 20, 2024, from https://polymer-additives.specialchem.com/selection-guide/nucleating-agents-selection-for-polypropylene.
31. Wu, Y., Hao, X., Lin, F., Wang, S., Chen, L., Lin, X., Gan, D., Fan, S., & Liu, Y. (2022). Developing a cerium lactate antibacterial nucleating agent for multifunctional polylactic acid packaging film. *International Journal of Biological Macromolecules*, *220*, 56–66.
32. Baimark, Y., & Kittipoom, S. (2018). Influence of chain-extension reaction on stereocomplexation, mechanical properties and heat resistance of compressed stereocomplex-polylactide bioplastic films. *Polymers*, *10*(11), 1218.
33. Yun, X., Li, X., Jin, Y., Sun, W., & Dong, T. (2018). Fast crystallization and toughening of poly (L-lactic acid) by incorporating with poly (ethylene glycol) as a middle block chain. *Polymer Science, Series A*, *60*, 141–155.
34. Srihanam, P., Pakkethati, K., Srisuwan, Y., Phromsopha, T., Manphae, A., Phinyocheep, P., ... & Baimark, Y. (2024). Utilization of bamboo biochar as a multi-functional filler of flexible poly(L–lactide)–*b*–poly(ethylene glycol)–*b*–poly (L–lactide) bioplastic. *Scientific Reports*, *14*(1), 17601.
35. Salimi, A., Ahmadi, S., Faramarzi, M., & Faghihi, J. (2023). Reactive blending of polylactic acid/polyethylene glycol toward biodegradable film. *Macromolecular Research*, *31*(9), 873–881.
36. Saeidlou, S., Huneault, M. A., Li, H., & Park, C. B. (2012). Poly(lactic acid) crystallization. *Progress in Polymer Science*, *37*(12), 1657–1677.
37. Shi, X., Zhang, G., Phuong, T. V., & Lazzeri, A. (2015). Synergistic effects of nucleating agents and plasticizers on the crystallization behavior of poly (lactic acid). *Molecules*, *20*(1), 1579–1593.
38. Tang, Z., Fan, F., Chu, Z., Fan, C., & Qin, Y. (2020). Barrier properties and characterizations of poly(lactic acid)/ZnO nanocomposites. *Molecules*, *25*(6), 1310.
39. Srisuwan, Y., Srihanam, P., Rattanasuk, S., & Baimark, Y. (2024). Preparation of Poly(L–lactide)–*b*–poly(ethylene glycol)–*b*–poly(L–lactide)/Zinc Oxide

Nanocomposite Bioplastics for Potential Use as Flexible and Antibacterial Food Packaging. *Polymers*, *16*(12), 1660.

40. Li, H., & Huneault, M. A. (2007). Effect of nucleation and plasticization on the crystallization of poly(lactic acid). *Polymer*, *48*(23), 6855–6866.
41. Wang, L., Wang, Y. N., Huang, Z. G., & Weng, Y. X. (2015). Heat resistance, crystallization behavior, and mechanical properties of polylactide/nucleating agent composites. *Materials & Design*, *66*, 7–15.
42. Chen, P., Yu, K., Wang, Y., Wang, W., Zhou, H., Li, H., & Wang, X. (2018). The effect of composite nucleating agent on the crystallization behavior of branched poly (lactic acid). *Journal of Polymers and the Environment*, *26*, 3718-3730.
43. Li, L., Cao, Z. Q., Bao, R. Y., Xie, B. H., Yang, M. B., & Yang, W. (2017). Poly (l–lactic acid)–polyethylene glycol–poly (l–lactic acid) triblock copolymer: a novel macromolecular plasticizer to enhance the crystallization of poly(l–lactic acid). *European Polymer Journal*, *97*, 272–281.
44. Li, Y., & Han, C. (2012). Isothermal and nonisothermal cold crystallization behaviors of asymmetric poly(L-lactide)/poly(D-lactide) blends. *Industrial & Engineering Chemistry Research*, *51*(49), 15927–15935.
45. Jalali, A., Huneault, M. A., & Elkoun, S. (2016). Effect of thermal history on nucleation and crystallization of poly(lactic acid). *Journal of Materials Science*, *51*, 7768-7779.
46. Gao, P., Alanazi, S., & Masato, D. (2024). Crystallization of polylactic acid with organic nucleating agents under quiescent conditions. *Polymers*, *16*(3), 320.
47. Ahmad, N. D., & Wildan, M. W. (2023). Preparation and properties of cellulose nanocrystals-reinforced poly(lactic acid) composite filaments for 3D printing applications. *Results in Engineering*, *17*, 100842.
48. Younus, M. M., Naguib, H. M., Fekry, M., & Elsawy, M. A. (2023). Pushing the limits of PLA by exploring the power of MWCNTs in enhancing thermal, mechanical properties, and weathering resistance. *Scientific Reports*, *13*(1), 16588.
49. Echeverría, C., Limón, I., Muñoz-Bonilla, A., Fernández-García, M., & López, D. (2021). Development of highly crystalline polylactic acid with β-crystalline phase from the induced alignment of electrospun fibers. *Polymers*, *13*(17), 2860.
50. Farahani, A., Zarei-Hanzaki, A., Abedi, H. R., Tayebi, L., & Mostafavi, E. (2021). Polylactic acid piezo-biopolymers: chemistry, structural evolution, fabrication methods, and tissue engineering applications. *Journal of Functional Biomaterials*, *12*(4), 71.
51. Zhang, H., Hortal, M., Jordá-Beneyto, M., Rosa, E., Lara-Lledo, M., & Lorente, I. (2017). ZnO-PLA nanocomposite coated paper for antimicrobial packaging application. *LWT*, *78*, 250–257.
52. Echeverría, C., Limón, I., Muñoz-Bonilla, A., Fernández-García, M., & López, D. (2021). Development of highly crystalline polylactic acid with β-crystalline

phase from the induced alignment of electrospun fibers. *Polymers*, *13*(17), 2860.

53. Bindhu, B., Renisha, R., Roberts, L., & Varghese, T. O. (2018). Boron nitride reinforced polylactic acid composites film for packaging: Preparation and properties. *Polymer Testing*, *66*, 172–177.
54. Pakkethati, K., Srihanam, P., Manphae, A., Rungseesantivanon, W., Prakymoramas, N., Lan, P. N., & Baimark, Y. (2024). Improvement in crystallization, thermal, and mechanical properties of flexible poly(L–lactide)–*b*–poly(ethylene glycol)–*b*–poly(L–lactide) Bioplastic with Zinc Phenylphosphate. *Polymers*, *16*(7), 975.
55. Abbas, M., Buntinx, M., Deferme, W., & Peeters, R. (2019). (Bio) polymer/ZnO nanocomposites for packaging applications: a review of gas barrier and mechanical properties. *Nanomaterials*, *9*(10), 1494.
56. Mohapatra, A. K., Mohanty, S., & Nayak, S. K. (2014). Dynamic mechanical and thermal properties of polylactide-layered silicate nanocomposites. *Journal of Thermoplastic Composite Materials*, *27*(5), 699–716.
57. Panicker, A. M., Rajesh, K. A., & Varghese, T. O. (2017). Mixed morphology nanocrystalline cellulose from sugarcane bagasse fibers/poly(lactic acid) nanocomposite films: synthesis, fabrication and characterization. *Iranian Polymer Journal*, *26*(2), 125–136.
58. Díez-Pascual, A. M., & Díez-Vicente, A. L. (2014). Poly(3–hydroxybutyrate)/ZnO bionanocomposites with improved mechanical, barrier and antibacterial properties. *International journal of molecular sciences*, *15*(6), 10950–10973.

# BIOGRAPHY

| | |
|---|---|
| **NAME** | Arriya Chuangchai |
| **DATE OF BIRTH** | 16/11/2000 |
| **PLACE OF BIRTH** | Ubon Ratchathani |
| **ADDRESS** | 8 Moo 8, Ban Nong Bua Luang, Som Sa-ard, Detudom, Ubon Ratchathani, 34160. Thailand |
| **POSITION** | Student |
| **PLACE OF WORK** | Mahasarakham University |
| **EDUCATION** | ¬ 2012–2017: High School Certificate equivalent, Detudom School, Detudom, Ubon Ratchathani, Thailand<br>¬ 2019–2022: Bachelor of Science, Mahasarakham University, Mahasarakham, Thailand<br>¬ 2022–Present: Master of Science Mahasarakham University, Mahasarakham, Thailand |
| **Research grants & awards** | Center of Excellence for Innovation in Chemistry |
| **Research output** | Chuangchai, A., & Baimark, Y. (2024). Improving crystallization properties, thermal stability, and mechanical properties of poly(L–lactide)–b–poly(ethylene glycol)–b–poly(L–lactide) bioplastic by incorporating cerium lactate. Polymers, 16(23), 3367. |